J-Researchers

Journal of Civil Engineering Researchers

Journal homepage: www.journals-researchers.com

Evaluation of the Effect of Rice husk ash on the Mechanical Properties and Gamma Ray Attenuation of Concrete

Shahin Charkhtab Moghaddam,[a,*] Morteza Jamshidi[b]

[a] *Department of Civil Engineering, Deylaman Institute of Higher Education, Iran.*

[b] *Department of Civil Engineering, Cha.C., Islamic Azad University, Chalus, Iran.*

ABSTRACT

This study investigated the viability of rice husk ash (RHA) as a sustainable and performance-enhancing partial substitute for cement in concrete. The used RHA, characterized by a novel chemical composition abundant in silicon and aluminum oxides, was incorporated into ordinary concrete at increasing substitution ratios up to 25%. A comprehensive evaluation was conducted to assess the influence of RHA on various properties of the resulting concrete, including physical (setting time, standard consistency, workability), mechanical (compressive and tensile strength), microstructural (XRD, and EDX), and radiation shielding characteristics. The results indicated that RHA marginally increased cement setting time, with a maximum 7.14% increase observed at a 25% replacement level. However, it significantly increased water demand for standard consistency, reaching 35.7% at 25% replacement. The increased water demand correlated with a reduction in workability, with a maximum slump reduction rate of 57.3% at the 25% replacement level. Importantly, the optimal replacement levels for mechanical strength enhancement were at 10% for compressive strength and 15% for tensile strength, achieving improvements of 13.74% and 9.48%, respectively. Additionally, The Monte Carlo simulation code as well as PhyX software were employed for assessing the concrete samples' significant gamma and fast neutron radiation attenuation characteristics. Gamma-ray attenuation tests demonstrated a modest improvement in the gamma-ray shielding capacity of the resulting concrete. The linear attenuation of the prepared sample containing 15% RHA was found to be higher than the other samples, due to its high density. On the contrary, the 25RHA sample is a less valuable sample. The 15RHA sample had the highest value for FCS (0.090 cm-1) indicating its efficacy and capability as a neutron shield.

ARTICLE INFO

Received: November 02, 2025
Accepted: December 14, 2025

Keywords:
Rice husk ash Equivalent Linear
Mechanical properties Scaled
Microstructure
Radiation shielding
Linear attenuation coefficient

DOI: 10.61186/JCER.8.2.15
DOR: 20.1001.1.22516530.1399.11.4.1.1

1. Introduction

Rising global temperatures provide compelling evidence of ongoing climate change, with carbon dioxide (CO_2) emissions widely recognized as a principal driving factor in this process. [1]. The construction industry represents a major contributor to global carbon emissions, thereby requiring focused research into robust mitigation pathways. Throughout the construction value chain, CO_2 is emitted during raw material extraction, mechanical and thermal processing, and the inherently carbon‐intensive production of cement. [2]. As an essential pillar of the construction and infrastructure industry, cement production encounters significant pressures, including

* Corresponding author. e-mail: charkhtab.shahin@iauc.ac.ir

diminishing fossil fuel reserves, limited raw material availability, escalating global demand, and increasing environmental scrutiny. With an estimated 7% share of global CO_2 emissions, the cement sector is recognized as a substantial contributor to climate change. The Intergovernmental Panel on Climate Change (IPCC) has identified carbon capture and storage (CCS) as a promising mitigation technology capable of reducing CO_2 emissions from cement manufacturing.[3].

CCS encompasses the capture of CO2 from point sources, such as cement kilns, its transportation via pipelines or other means, and its long-term geological storage in suitable formations, such as depleted oil and gas reservoirs, thereby preventing its release into the atmosphere. However, the widespread deployment of CCS is currently hindered by significant economic barriers, including high capital and operational costs, and substantial energy requirements for capture and compression, which can reduce the overall efficiency of the industrial process[4].Biochar is a carbon-rich solid material, produced via thermochemical conversion (pyrolysis) of biomass under oxygen-limited conditions, offering a promising avenue for carbon sequestration [5]. Its highly porous structure and recalcitrant nature enable the long-term stabilization of carbon, effectively removing it from the active carbon cycle. Biochar is widely used as an environmentally friendly material in a variety of applications. For instance, wood-based biochar is commonly used for wastewater treatment for removing heavy metals and carbon sequestration due to its high carbon content and porous structure [6], while rice husk ash is widely applied as a soil amendment [7] and as a supplementary cementitious material in concrete. Corn cob biochar is often utilized as a soil ameliorant, as well as in fuel cells and bio composites material [8], whereas bamboo biochar, known for its excellent adsorptive properties, is ideal for air and water purification systems [9]. Similarly, coconut shell biochar is frequently employed in biodiesel production and capacitive deionization [10]. These diverse types of biochar cater to a wide range of industrial, agricultural, and environmental applications, highlighting their versatility and importance.

Incorporating biochar into cementitious materials offers a dual benefit: it reduces the embodied carbon footprint of concrete by partially replacing cement clinker, a major source of CO2 emissions, and can also enhance certain properties, such as workability, strength, and durability, depending on the biochar feedstock, production conditions, and incorporation rate [11]. While some studies report improvements in compressive strength, others observe a decrease, highlighting the importance of optimizing biochar properties and mix design [12]. The physicochemical properties of biochar, including elemental composition, stability, surface area, and functional groups, are significantly influenced by its origin and processing conditions (eg. pyrolysis temperature) [13]. The chemical composition of biochar—predominantly carbon, hydrogen, oxygen, nitrogen, and sulfur, with trace minerals such as potassium, phosphorus, and calcium—is fundamentally dictated by the feedstock characteristics and the specific pyrolysis parameters. As a thermal degradation process occurring under oxygen-limited conditions, pyrolysis parameters like temperature and heating rate are key determinants of biochar's final properties. Specifically, low-temperature pyrolysis (typically 300–450 °C) yields biochar characterized by a higher volatile matter content and a less developed aromatic framework. These materials typically exhibit higher H/C and O/C molar ratios, reflecting a predominantly aliphatic nature Conversely, [14]pyrolysis at higher temperatures (above 600 °C) promotes greater carbonization and the formation of more condensed aromatic structures.

As a result, biochars produced under these conditions typically exhibit higher fixed carbon content, increased porosity, larger surface area, and a greater degree of ordered graphitic domain development. In addition, the H/C and O/C molar ratios decrease with rising pyrolysis temperature, indicating the progressive loss of hydrogen- and oxygen-containing functional groups [15].This structural variability, which can range from relatively amorphous to more graphitic forms, sets biochar apart from the highly ordered crystalline structure of graphene. This distinction is essential for understanding biochar's wide range of applications, since variations in structure lead to differences in properties such as adsorption, reactivity, and stability[16].

The use of diverse biochar types in concrete has been the subject of numerous investigations, with a focus on their impact on physical, mechanical, and microstructural characteristics. Table 1 presents the key findings of several studies on the various properties of concrete.This study introduces a novel rice husk ash as a potential concrete admixture. The key innovation is the biochar's unique chemical composition, characterized by a substantially higher content of silicon and aluminum oxides, exceeding 43% by the total weight and approximately 92% of the mineral weight.

This contrasts sharply with conventional rice husk ash s used in previous research, where these oxides constituted less than 20% [17-19]. This elevated silicon and aluminum oxide content is expected to enhance the concrete's pozzolanic activity, leading to improved strength, durability, and microstructure. Beyond the unique chemical composition of the RHA, this study's novelty lies also in the comprehensive investigation of the resulting concrete's radiation shielding properties to provide novel insights into fast neutrons and gamma ray attenuation behavior of RHA-amended concrete.

Table 1.
Properties of concrete incorporating various types of biochar powders in literature studies.

Reference	Biochar type	Optimum replacement / addition ratio	Main conclusions	Other notes
Akhtar& Sarmah (2018) [1]	Pulp and paper mill residues Rice husk	0.1% of the total volume.	A growing body of research has demonstrated that biochar can substantially enhance the mechanical and durability performance of cementitious materials, although the magnitude and direction of improvement depend on biochar type, particle size, and dosage. At early ages, compressive strength improvements of 10% and 6% were reported with pulp-and-paper mill biochar and rice husk ash (RHA), respectively, while flexural strength increased by up to 20% with the incorporation of poultry litter or RHA at a 0.1% dosage. Wood-derived biochar at 0.5 wt% yielded notable compressive strength enhancements of 17% at 7 days and 16% at 28 days, and at higher dosages of 1–2 wt% it also mitigated thermal degradation, achieving 20% higher strength retention upon exposure to elevated temperatures. Similarly, wheat straw biochar improved both strength and durability: mortars containing 0.5–1.5 wt% showed compressive strength gains of 4.1–17.3%, a 9% increase in flexural strength, and substantial reductions in sorptivity (33.8%) and water absorption (25%).	The incorporation of rice husk ash (RHA) at a concentration of 0.1% produced a slight increase in splitting tensile strength, while also contributing to a modest reduction in production costs through partial cement substitution. In terms of thermal resistance, concrete containing 2% biochar exhibited up to a 45% improvement in impermeability after exposure to 550 °C. Similarly, the addition of 1% biochar enhanced water tightness, reducing capillary absorption and water penetration by 28% and 43%, respectively, relative to the control mix. Energy-dispersive spectroscopy (EDS) of wheat-straw-biochar mortars suggested the potential formation of additional hydration products, consistent with observed reductions of 30% and 31% in total and permeable air void volumes at a 1.5% dosage.
Gupta et al (2020) [19]	Wood waste	0.5% of cement weight.	Biochar contents between 2 wt% and 6.5 wt% have frequently yielded optimal strength improvements. For example, 2 wt% bagasse biochar increased compressive strength by 18%, attributed to its high silica content (16.62%) and fine particle size, while 6.5 wt% biochar produced compressive strength gains of 32.9% and 35.2% at 7 and 28 days, respectively. However, exceeding the optimal dosage often resulted in reduced splitting tensile strength or diminishing returns. Long-term studies further showed that 2 wt% biochar improved compressive strength by 3%, 7%, and 9% at curing ages of 28 days, 1 year, and 2 years, respectively, with additional reductions in sorptivity and water absorption linked to internal densification effects.	Biochar dosage had varying effects on water absorption: while optimal amounts reduced sorptivity and improved microstructure through particle densification, increases in biochar content were also associated with higher overall water absorption. Comparative evaluation of different biochars showed that their effectiveness in modifying cementitious materials followed the order: bagasse > rice husk > peanut husk > coconut husk > wheat husk. The reduction in water absorption and sorptivity was consistent with decreased workability at higher biochar contents, attributable to the hydrophilic and porous nature of the material.
Ahmad et al (2020) [20]	Wheat straw	1.5% of cement weight.	Biochar also enhances microstructural development. XRD, SEM, FTIR, EDX, and Raman analyses have consistently confirmed increased formation of hydration products, improved matrix densification, and reduced pore connectivity. In bamboo biochar mortars, the high silicon and aluminum oxide content imparted a pozzolanic effect, resulting in a 32.9% increase in early-age strength and improved crack resistance at 1–3 wt% replacement. Wood-waste biochar with increased fineness produced optimal reductions in carbonation depth (17.9%) and chloride diffusion (32%) at 1–3 wt%, while simultaneously increasing compressive strength by 18.48%. Likewise, corn straw biochar at 1 wt% increased compressive strength by 5.3%, and at 3 wt% improved peak load by up to 11.4% and initial fracture toughness by as much as 46.8% across multiple curing ages.	Specific biochar types demonstrated specialized functional benefits. For example, bamboo biochar exhibited a strong pozzolanic effect due to its high silicon and aluminum oxide content. A 1 wt% replacement was identified as optimal for maximizing crack resistance, while dosages between 1% and 3% consistently improved compressive strength and fracture toughness through filling and self-curing effects. Wood-waste biochar at a 3% replacement level enhanced cement hydration and microstructure by providing nucleation sites and filling internal pores, as evidenced by SEM and XRD analyses. However, biochar incorporation also reduced ductility and fracture energy; a 3 wt% addition decreased fracture energy by 3.6%, 33.3%, and 33.2% at 7, 14, and 28 days, respectively.

Continued on next page

Reference	Biochar type	Optimum replacement / addition ratio	Main conclusions	Other notes
Qin et al (2021) [21]	Synthetic eucalyptus plywood	6.5% of cement weight.	Durability performance also benefits from biochar incorporation. After exposure to temperatures of 300–700 °C, mixtures containing 3% RHA exhibited residual strength increases of 4.8%, 26.3%, and 25%, respectively. Concrete with 2 wt% biochar showed up to 45% improved impermeability after heating to 550 °C, and 1 wt% biochar reduced capillary absorption and water penetration by 28% and 43%. Biochars with strong pozzolanic characteristics, such as alum sludge biochar, further improved durability: the 5% replacement achieved a compressive strength of 31 MPa and reduced global warming potential by 32.2%. Across 16 different biochar types, milled biochars used at 10% replacement often matched or exceeded control strengths, with white hardwood biochar outperforming the control by more than 48%.	Biochar also influenced fresh properties. Increasing its dosage raised the water demand for normal consistency and shortened setting time, with large replacements (e.g., 30%) resulting in minimal slump and sharply reduced plasticity. Nevertheless, the optimal RHA content of 3 wt% enhanced micro-filling and secondary hydration, increasing 28-day compressive, splitting tensile, and flexural strengths by 9.9%, 7.2%, and 6.8%, respectively. The pozzolanic reactivity of alum-sludge biochar was likewise confirmed analytically. Moreover, studies showed that a wide range of milled biochars can effectively replace up to 10% of cement without compromising strength.
Javed et al (2022) [18]	Bagasse Coconut husk Peanut husk Rice husk Wheat husk	2% of cement weight.	In engineered cementitious composites, the incorporation of 10–20 wt% biochar increased tensile strain capacity and reduced crack width despite causing a moderate (~10%) reduction in compressive strength. However, this trade-off is accompanied by significant sustainability benefits, including up to 58.3% reductions in carbon emissions and lower production costs due to reduced cement use and potential carbon-tax savings.	In broader sustainability assessments, incorporating biochar reduced total and specific carbon emissions by as much as 58.3%, while lowering production costs due to reduced cement consumption and potential carbon-tax savings. These combined mechanical, durability, and environmental benefits demonstrate that biochar additions of 10–20% can offer a cost-effective, sustainable, and structurally reliable alternative for modern construction applications.
Sirico et al (2022) [22]	Forestry waste residues	2% of cement weight.	Overall, the literature demonstrates consistent evidence that biochar—across diverse feedstocks and processing conditions—can improve the mechanical performance, durability, microstructure, and sustainability profile of cementitious materials when used at appropriate dosages, typically between 1% and 6%.	The incorporation of rice husk ash (RHA) at a concentration of 0.1% produced a slight increase in splitting tensile strength, while also contributing to a modest reduction in production costs through partial cement substitution. In terms of thermal resistance, concrete containing 2% biochar exhibited up to a 45% improvement in impermeability after exposure to 550 °C. Similarly, the addition of 1% biochar enhanced water tightness, reducing capillary absorption and water penetration by 28% and 43%, respectively, relative to the control mix. Energy-dispersive spectroscopy (EDS) of wheat-straw-biochar mortars suggested the potential formation of additional hydration products, consistent with observed reductions of 30% and 31% in total and permeable air void volumes at a 1.5% dosage.
Liu et al (2022) [23]	Bamboo biochar	4% of cement weight.	A growing body of research has demonstrated that biochar can substantially enhance the mechanical and durability performance of cementitious materials, although the magnitude and direction of improvement depend on biochar type, particle size, and dosage. At early ages, compressive strength improvements of 10% and 6% were reported with pulp-and-paper mill biochar and rice husk ash (RHA), respectively, while flexural strength increased by up to 20% with the incorporation of poultry litter or RHA at a 0.1% dosage. Wood-derived biochar at 0.5 wt% yielded notable compressive strength enhancements of 17% at 7 days and 16% at 28 days, and at higher dosages of 1–2 wt% it also mitigated	Biochar dosage had varying effects on water absorption: while optimal amounts reduced sorptivity and improved microstructure through particle densification, increases in biochar content were also associated with higher overall water absorption. Comparative evaluation of different biochars showed that their effectiveness in modifying cementitious materials followed the order: bagasse > rice husk > peanut husk > coconut husk > wheat husk. The reduction in water absorption and sorptivity was consistent with decreased workability at higher biochar contents, attributable to the hydrophilic and porous nature of the material.

Continued on next page

Reference	Biochar type	Optimum replacement / addition ratio	Main conclusions	Other notes
			thermal degradation, achieving 20% higher strength retention upon exposure to elevated temperatures. Similarly, wheat straw biochar improved both strength and durability: mortars containing 0.5–1.5 wt% showed compressive strength gains of 4.1–17.3%, a 9% increase in flexural strength, and substantial reductions in sorptivity (33.8%) and water absorption (25%).	
Ling et al (2023) [24]	Wood waste	3% of cement weight.	Biochar contents between 2 wt% and 6.5 wt% have frequently yielded optimal strength improvements. For example, 2 wt% bagasse biochar increased compressive strength by 18%, attributed to its high silica content (16.62%) and fine particle size, while 6.5 wt% biochar produced compressive strength gains of 32.9% and 35.2% at 7 and 28 days, respectively. However, exceeding the optimal dosage often resulted in reduced splitting tensile strength or diminishing returns. Long-term studies further showed that 2 wt% biochar improved compressive strength by 3%, 7%, and 9% at curing ages of 28 days, 1 year, and 2 years, respectively, with additional reductions in sorptivity and water absorption linked to internal densification effects.	Specific biochar types demonstrated specialized functional benefits. For example, bamboo biochar exhibited a strong pozzolanic effect due to its high silicon and aluminum oxide content. A 1 wt% replacement was identified as optimal for maximizing crack resistance, while dosages between 1% and 3% consistently improved compressive strength and fracture toughness through filling and self-curing effects. Wood-waste biochar at a 3% replacement level enhanced cement hydration and microstructure by providing nucleation sites and filling internal pores, as evidenced by SEM and XRD analyses. However, biochar incorporation also reduced ductility and fracture energy; a 3 wt% addition decreased fracture energy by 3.6%, 33.3%, and 33.2% at 7, 14, and 28 days, respectively.
Qing et al (2023) [25]	Corn straw	1-3% of cement weight.	Biochar also enhances microstructural development. XRD, SEM, FTIR, EDX, and Raman analyses have consistently confirmed increased formation of hydration products, improved matrix densification, and reduced pore connectivity. In bamboo biochar mortars, the high silicon and aluminum oxide content imparted a pozzolanic effect, resulting in a 32.9% increase in early-age strength and improved crack resistance at 1–3 wt% replacement. Wood-waste biochar with increased fineness produced optimal reductions in carbonation depth (17.9%) and chloride diffusion (32%) at 1–3 wt%, while simultaneously increasing compressive strength by 18.48%. Likewise, corn straw biochar at 1 wt% increased compressive strength by 5.3%, and at 3 wt% improved peak load by up to 11.4% and initial fracture toughness by as much as 46.8% across multiple curing ages.	Biochar also influenced fresh properties. Increasing its dosage raised the water demand for normal consistency and shortened setting time, with large replacements (e.g., 30%) resulting in minimal slump and sharply reduced plasticity. Nevertheless, the optimal RHA content of 3 wt% enhanced micro-filling and secondary hydration, increasing 28-day compressive, splitting tensile, and flexural strengths by 9.9%, 7.2%, and 6.8%, respectively. The pozzolanic reactivity of alum-sludge biochar was likewise confirmed analytically. Moreover, studies showed that a wide range of milled biochars can effectively replace up to 10% of cement without compromising strength.
Jia et al (2023) [26]	Municipal solid waste	1-10% of cement weight.	Durability performance also benefits from biochar incorporation. After exposure to temperatures of 300–700 °C, mixtures containing 3% RHA exhibited residual strength increases of 4.8%, 26.3%, and 25%, respectively. Concrete with 2 wt% biochar showed up to 45% improved impermeability after heating to 550 °C, and 1 wt% biochar reduced capillary absorption and water penetration by 28% and 43%. Biochars with strong pozzolanic characteristics, such as alum sludge biochar, further improved durability: the 5% replacement achieved a compressive strength of 31 MPa and reduced global warming potential by 32.2%. Across 16 different biochar types, milled biochars used at 10% replacement often matched or exceeded control strengths, with white hardwood biochar outperforming the control by more than 48%.	In broader sustainability assessments, incorporating biochar reduced total and specific carbon emissions by as much as 58.3%, while lowering production costs due to reduced cement consumption and potential carbon-tax savings. These combined mechanical, durability, and environmental benefits demonstrate that biochar additions of 10–20% can offer a cost-effective, sustainable, and structurally reliable alternative for modern construction applications.

Continued on next page

Reference	Biochar type	Optimum replacement / addition ratio	Main conclusions	Other notes
Pang et al (2024) [27]	Waste synthetic eucalyptus plywood boards	3% of cement weight.	In engineered cementitious composites, the incorporation of 10–20 wt% biochar increased tensile strain capacity and reduced crack width despite causing a moderate (~10%) reduction in compressive strength. However, this trade-off is accompanied by significant sustainability benefits, including up to 58.3% reductions in carbon emissions and lower production costs due to reduced cement use and potential carbon-tax savings.	The incorporation of rice husk ash (RHA) at a concentration of 0.1% produced a slight increase in splitting tensile strength, while also contributing to a modest reduction in production costs through partial cement substitution. In terms of thermal resistance, concrete containing 2% biochar exhibited up to a 45% improvement in impermeability after exposure to 550 °C. Similarly, the addition of 1% biochar enhanced water tightness, reducing capillary absorption and water penetration by 28% and 43%, respectively, relative to the control mix. Energy-dispersive spectroscopy (EDS) of wheat-straw-biochar mortars suggested the potential formation of additional hydration products, consistent with observed reductions of 30% and 31% in total and permeable air void volumes at a 1.5% dosage.
Mekky et al (2024) [28]	Alum sludge	5% of cement weight.	Overall, the literature demonstrates consistent evidence that biochar—across diverse feedstocks and processing conditions—can improve the mechanical performance, durability, microstructure, and sustainability profile of cementitious materials when used at appropriate dosages, typically between 1% and 6%.	Biochar dosage had varying effects on water absorption: while optimal amounts reduced sorptivity and improved microstructure through particle densification, increases in biochar content were also associated with higher overall water absorption. Comparative evaluation of different biochars showed that their effectiveness in modifying cementitious materials followed the order: bagasse > rice husk > peanut husk > coconut husk > wheat husk. The reduction in water absorption and sorptivity was consistent with decreased workability at higher biochar contents, attributable to the hydrophilic and porous nature of the material.
Hylton et al (2024) [29]	16 various biochar types	10% of cement weight.	A growing body of research has demonstrated that biochar can substantially enhance the mechanical and durability performance of cementitious materials, although the magnitude and direction of improvement depend on biochar type, particle size, and dosage. At early ages, compressive strength improvements of 10% and 6% were reported with pulp-and-paper mill biochar and rice husk ash (RHA), respectively, while flexural strength increased by up to 20% with the incorporation of poultry litter or RHA at a 0.1% dosage. Wood-derived biochar at 0.5 wt% yielded notable compressive strength enhancements of 17% at 7 days and 16% at 28 days, and at higher dosages of 1–2 wt% it also mitigated thermal degradation, achieving 20% higher strength retention upon exposure to elevated temperatures. Similarly, wheat straw biochar improved both strength and durability: mortars containing 0.5–1.5 wt% showed compressive strength gains of 4.1–17.3%, a 9% increase in flexural strength, and substantial reductions in sorptivity (33.8%) and water absorption (25%).	Specific biochar types demonstrated specialized functional benefits. For example, bamboo biochar exhibited a strong pozzolanic effect due to its high silicon and aluminum oxide content. A 1 wt% replacement was identified as optimal for maximizing crack resistance, while dosages between 1% and 3% consistently improved compressive strength and fracture toughness through filling and self-curing effects. Wood-waste biochar at a 3% replacement level enhanced cement hydration and microstructure by providing nucleation sites and filling internal pores, as evidenced by SEM and XRD analyses. However, biochar incorporation also reduced ductility and fracture energy; a 3 wt% addition decreased fracture energy by 3.6%, 33.3%, and 33.2% at 7, 14, and 28 days, respectively.
Wang et al (2025) [30]	Peanut shell-based biomass	10-20% of cement weight.	Biochar contents between 2 wt% and 6.5 wt% have frequently yielded optimal strength improvements. For example, 2 wt% bagasse biochar increased compressive strength by 18%, attributed to its high silica content (16.62%) and fine particle size, while 6.5 wt% biochar produced compressive strength gains of 32.9% and 35.2% at 7 and 28 days,	Biochar also influenced fresh properties. Increasing its dosage raised the water demand for normal consistency and shortened setting time, with large replacements (e.g., 30%) resulting in minimal slump and sharply reduced plasticity. Nevertheless, the optimal RHA

Continued on next page

Reference	Biochar type	Optimum replacement / addition ratio	Main conclusions	Other notes
			respectively. However, exceeding the optimal dosage often resulted in reduced splitting tensile strength or diminishing returns. Long-term studies further showed that 2 wt% biochar improved compressive strength by 3%, 7%, and 9% at curing ages of 28 days, 1 year, and 2 years, respectively, with additional reductions in sorptivity and water absorption linked to internal densification effects.	content of 3 wt% enhanced micro-filling and secondary hydration, increasing 28-day compressive, splitting tensile, and flexural strengths by 9.9%, 7.2%, and 6.8%, respectively. The pozzolanic reactivity of alum-sludge biochar was likewise confirmed analytically. Moreover, studies showed that a wide range of milled biochars can effectively replace up to 10% of cement without compromising strength.

2. Materials Properties

2.1. Cement

In this study, Type I Ordinary Portland Cement (OPC) with a 42.5 N strength grade, conforming to ASTM C150 [31], was utilized. This OPC was sourced from Wadi El-Nile cement company. The physical and mechanical properties of the OPC are detailed in Table 2, while its chemical composition, determined via X-Ray Fluorescence (XRF) analysis, is presented in Table 3. Specific gravity was determined according to ASTM C188 [32]. The initial and final setting times, along with standard consistency, were evaluated using a Vicat apparatus (Figure 1(a)). Soundness was assessed using a Le Chatelier apparatus (Figure 1(b)) following BS EN 196-3:2005 [33]. Compressive strength testing was performed after 28 days of curing, in accordance with ASTM C109/C109M-11 [34], to verify the mechanical performance of the resulting concrete. Particle size distribution of the OPC, determined using laser scattering particle size analysis, is illustrated in Figure 1(c), revealing a mean particle size of approximately 9 μm. Mineralogical and microstructural characterization was conducted using X-ray diffraction (XRD) with the results presented in Figures 1(d). XRD analysis revealed the presence of the principal crystalline phases in Portland cement clinker: alite (C3S), belite (C2S), tricalcium aluminate (C3A), tetracalcium aluminoferrite (C4AF), and gypsum. This mineralogical profile, consistent with the chemical composition determined by XRF, demonstrates that the cement's composition is in accordance with the expected mineralogy for its type, thereby confirming its quality and compliance with relevant industry standards.

2.2. Aggregates

Natural siliceous sand, sampled in accordance with ASTM D75 [35], served as the fine aggregate in this study. Particle size distribution was determined through sieve analysis following ASTM C136 [34] to verify compliance with design specifications and standard limits. The results of the sieve analysis are presented in Figure 2(a). The calculated Fineness Modulus (FM) of 2.47 indicates a typical mean particle size, consistent with ASTM C33 requirements. The physical properties of the fine aggregate are summarized in Table 4. For coarse aggregates, crushed dolomite with a nominal maximum size 19 mm was used as the coarse aggregate in all concrete mixes. Gradation testing, essential for design compliance and adherence to standard limits, was performed using sieve analysis according to ASTM C136 [36], as shown in Figure 2(b). The physical properties of the coarse aggregate are summarized in Table 4. The crushing value was determined according to BS 812 Part 110 [37]. ASTM C128 [38]was used to determine specific gravity and absorption. Bulk density and voids content were measured according to ASTM C29 [39]. The content of fine materials was assessed according to ASTM C142 [40]. The procedures employed for determining the physical properties of the coarse aggregate are illustrated in Figures 2(c, d).

2.3. Water and superplasticizer

[Clean potable water conforming to the standards outlined in ASTM C1602/C1602M [41], was used for concrete specimen mixing and curing. On the other hand, biochar particles exhibit a high porosity and water absorption capacity, which can significantly affect the workability of concrete mixtures. The high porosity of biochar leads to increased water absorption, reducing the available free water in the mix and thus lowering concrete fluidity. To address this challenge and enhance workability, the addition of chemical admixtures, specifically superplasticizers (SP), is essential. These admixtures improve the distribution of biochar particles within the mix and counteract the negative effects of water absorption. A commercially available SP, Sikament NN, supplied by the Egyptian branch of Sika Company, was incorporated during mixing at a constant dosage of 1.05% by weight of water. This SP meets the requirements for Type (F) chemical admixtures as specified in ASTM C494 [42]. Key characteristics of the SP are presented in

Table 5. The inclusion of the SP was driven by concerns over the potential difficulty in achieving a uniform concrete mixture and the expected reduction in workability due to biochar's high-water absorption. Furthermore, the relatively low water-to-cement (w/c) ratio employed could also negatively impact mixture workability. Figure 3 shows the appearance of the used mixing and curing water in addition to the used SP.

2.4. Rice husk ash (RHA)

Biochar is a carbon‐rich material produced through the pyrolysis of organic biomass under oxygen‐limited conditions. During this thermochemical process, agricultural residues, wood chips, manure, or other lignocellulosic materials are heated to elevated temperatures, causing devolatilization and leaving behind a stable, carbon‐rich solid. The physicochemical properties of biochar are strongly influenced by the feedstock type and pyrolysis parameters, including temperature, heating rate, and residence time. Owing to its high carbon content and long-term stability, biochar offers substantial environmental benefits, particularly in carbon sequestration, reduction of greenhouse gas emissions, and climate change mitigation.

In this study, rice husk ash (RHA) is examined to assess its effects on the physical, mechanical, and—importantly for the first time—radiation‐shielding properties of concrete. RHA, shown after grinding in Figure 4(a), is derived from the pyrolysis of rice husks, an abundant byproduct of rice milling. The rice husk feedstock was pyrolyzed at temperatures exceeding 600 °C using a pilot‐scale continuous pyrolysis unit. The resulting biochar was subsequently analyzed by Eurofins Laboratories, an institution accredited under the European Biochar Certificate (ERHA). The comprehensive analysis included ultimate analysis (CHNSO) to determine organic carbon content and calculate H/C and O/C molar ratios as indicators of carbon stability. Additional parameters such as ash content, moisture content, trace metal concentrations, and polycyclic aromatic hydrocarbon (PAH) levels were also evaluated. A complete summary of the analytical results is presented in Appendix 1, detailing the methods used, ERHA reference thresholds, and results on both an as‐received and dry basis.

The RHA used in this study contains 44.8% organic carbon (dry basis) and exhibits good carbon stability, as reflected by an H/C_org ratio of 0.23. Although the ash content is relatively high (49.9%) compared with biochars derived from woody feedstocks, this characteristic is advantageous for construction applications due to its mineralogical composition. No ERHA‐based threshold limits apply to trace metals when biochar is used in construction materials, and the measured concentrations confirm that this RHA is suitable for building applications. PAH analysis further supports its suitability: the total concentration of the 16 EPA PAHs was only 2.2 mg/kg, and no detectable contamination was observed for the 8 EPA priority PAHs, benzo(e)pyrene, or benzo(j)fluoranthene.

The RHA employed in this investigation is characterized by a high silica content (Table 6), a porous microstructure, and a bulk density of approximately 1.3 g/cm³. Its pozzolanic reactivity makes it an effective partial cement substitute, with the material containing 43.2% silicon and aluminum oxides—equivalent to 92.37% of the mineral fraction of the ash when excluding carbon dioxide. These pozzolanic constituents react with calcium hydroxide in the cement matrix to form additional calcium–silicate–hydrate (C‐S‐H), thereby improving concrete strength and durability. Moreover, the high surface area and internal porosity of RHA enhance water retention, reduce permeability, and potentially increase resistance to cracking and environmental degradation. The use of RHA also contributes to sustainability by valorizing agricultural waste and reducing dependence on Portland cement.

Despite these advantages, several challenges remain. The quality of RHA can vary depending on the feedstock and pyrolysis conditions, influencing workability, consistency, and mechanical performance. High biochar contents may reduce workability due to increased water demand, making the use of superplasticizers or other admixtures necessary. The particle size distribution of the RHA used here is presented in Figure 4(b), with an average particle size of 17.5 µm. X‐ray diffraction analysis (Figure 4©) demonstrates the predominantly amorphous nature of the material. The broad diffraction band between $2\theta = 15°$ and 25° corresponds to amorphous carbon with randomly oriented aromatic layers, consistent with observations reported by Dehkhoda et al. (2014).[43]. Additionally, the low intensity sharp peaks correspond to miscellaneous inorganic components identified by quartz, graphite and coquimbite minerals, where the coquimbite is a secondary sulfate mineral which occurs due to oxidation process of iron sulfide and crystallized during the biochar production process.

3. Experimental program and test setup.

3.1. Preliminary compressive strength test on RHA mortar

A preliminary compressive strength assessment was performed on 50 × 50 × 50 mm cement mortar cubes (Figure 5) at a curing age of 28 days to evaluate the feasibility of the selected RHA replacement ratios prior to

their use as partial cement substitutes in concrete. The mortar mixtures were prepared in accordance with ASTM C109/C109M, using a cement to sand ratio of 1:2.75 by weight and a water to cement ratio of 0.485. As shown in Figure 6, the highest compressive strength was achieved at a 15% RHA replacement level, corresponding to an 8.71% increase relative to the control specimen. However, replacement levels exceeding 20% adversely affected strength development; at 25% substitution, the compressive strength decreased by 2.07% compared to the control mix. These findings confirm that the selected RHA replacement ratios are appropriate for subsequent incorporation into concrete mixtures.

3.2. Concrete mix design

The experimental program was designed to develop and evaluate ordinary concrete mixtures to investigate the mechanical, physical, and radiation shielding performance of rice husk ash (RHA) when used as a partial cement replacement. All concrete mixtures were proportioned according to the ACI 211.1 methodology to ensure consistency and reliable comparison among mixes. For the control mixture, the material quantities per cubic meter (1 m^3) were 380 kg of cement, 1190 kg of coarse aggregate, 720 kg of fine aggregate, and 142.5 kg of water, as detailed in Table 7. A water to cement (w/c) ratio of 0.375 was selected to achieve an appropriate balance between strength and workability. Additionally, a superplasticizer (SP) dosage of approximately 1.05% by water weight was incorporated to enhance mixture fluidity and ensure adequate homogeneity during casting.

RHA was incorporated into the concrete at five progressively increasing replacement levels, up to a maximum of 25%, enabling a systematic assessment of its influence on concrete performance. The selected range of substitution ratios is consistent with recent research investigating higher biochar based replacement levels in cementitious composites.[29, 30].

The use of higher RHA substitution rates is supported by the increasing recognition of biochar as a multifunctional, sustainability enhancing material. As a biomass derived product, biochar contributes to carbon sequestration: atmospheric carbon fixed during plant growth becomes stabilized through pyrolysis, enabling long term carbon storage when incorporated into concrete. Its utilization also promotes waste valorization, since materials such as rice husks—commonly disposed of or openly burned—are converted into value added products, thereby reducing environmental pollution and supporting circular economy initiatives.

Nevertheless, the mechanical and physical performance of concrete incorporating RHA must be carefully optimized. Elevated replacement levels can negatively affect strength and workability due to the material's high surface area, increased water absorption, and reduced effective binder content. Accordingly, the present experimental program sought to balance the sustainability advantages of higher RHA substitution with the need to maintain acceptable fresh and hardened concrete properties.

3.3. Specimens' preparation and curing

To evaluate the mechanical performance of concrete incorporating rice husk ash (RHA), compressive and tensile strength tests were performed on specimens of standard laboratory dimensions. For compressive strength determination, concrete cubes measuring $100 \times 100 \times 100$ mm were cast, while cylindrical specimens with a diameter of 100 mm and a height of 200 mm were prepared for tensile strength testing.

The mixing procedure was designed to ensure uniform material dispersion and consistency across all mixtures. Coarse and fine aggregates were first blended for two minutes, after which cement and RHA were added and mixed for an additional two minutes. The predetermined quantity of water, incorporating the liquid superplasticizer (SP), was then introduced, and mechanical mixing continued for a further three minutes to achieve proper homogenization.

Immediately after casting, the mixtures were compacted using a mechanical vibrator to eliminate air voids and ensure surface uniformity. The specimens remained in their molds for 24 hours before being demolded and placed in a curing tank containing potable water at ambient temperature and a relative humidity of at least 90%. Curing was maintained for approximately 27 days.

Following curing, all specimens were removed and oven dried at 105 °C for two hours to eliminate residual moisture before being subjected to gamma radiation attenuation testing. Mechanical property measurements were subsequently performed on the same specimens the day after completion of the radiation shielding experiments.

3.4. Tests setup

3.4.1. Physical properties of fresh concrete

To elucidate the impact of incorporating rice husk ash (RHA) biochar as a partial cement substitute, the fresh properties of the concrete mixtures were systematically evaluated and compared against a control mix. The investigation focused on standard consistency, initial and final setting times, and slump performance, providing a

comprehensive assessment of the material's influence on concrete workability and rheological behavior.

Owing to the highly porous microstructure of biochar, which typically increases water demand and absorption, its inclusion can significantly alter the effective water-to-cement ratio and the rate of hydration. Consequently, this study addresses these factors to clarify how biochar modifies the fresh-state characteristics and to determine its implications for practical construction applications.

Standard consistency—representing the water content required for a cement paste to reach a specified degree of stiffness—and setting times—which mark the duration required for the paste to achieve defined levels of rigidity—were determined using a Vicat needle apparatus. These measurements were conducted in accordance with ASTM C191 guidelines. Additionally, the workability of the concrete mixtures was assessed via the slump test to evaluate the effect of RHA replacement levels on the fluidity and consistency of the fresh concrete. [44]. On the other hand, the slump cone test was conducted in accordance with the procedures specified in ASTM C143/C143M [45]. This test employed a standard slump cone with a height of 300 mm, a top diameter of 100 mm, and a base diameter of 200 mm.

(a)

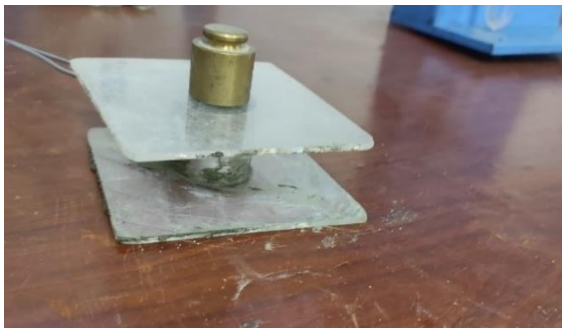

(b)

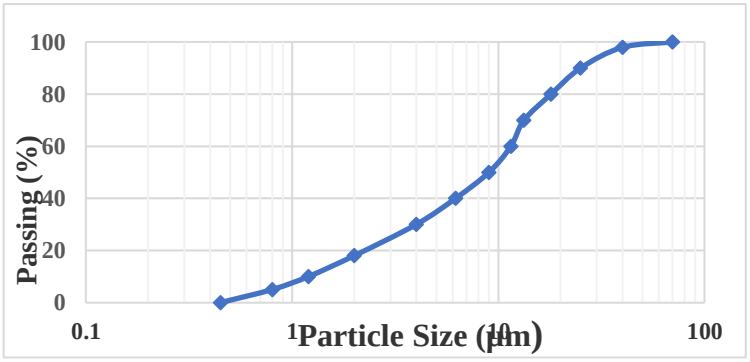

(c)

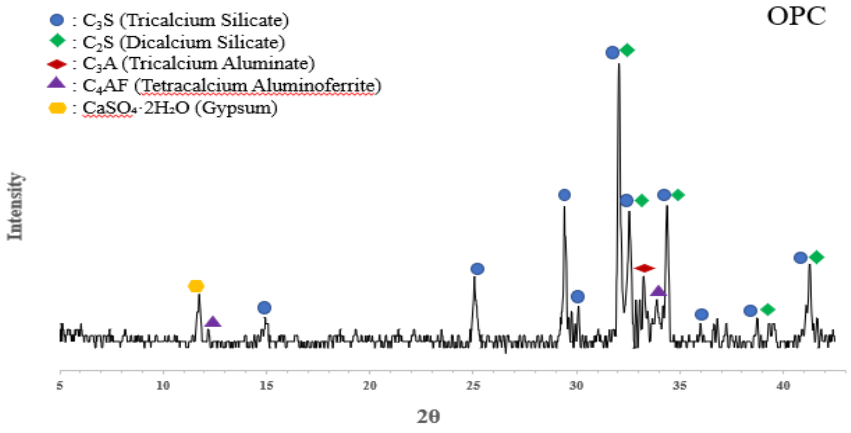

(d)

Figure 1: (a) Vicat apparatus, (b) le chatelier instrument, (c) particle size distribution of cement, (d) XRD pattern of the used cement.

Table 2.
Properties of used cement

Physical properties							Mortar compressive strength (MPa)		
Color	Specific gravity	Initial setting time (min)	Final setting time (min)	Surface area(cm^2/g)	Standard consistency (w/c%)	Soundness (mm)	3 days	7 days	28 days
Grey	3.16	120	210	3550	28%	1	25	33	43

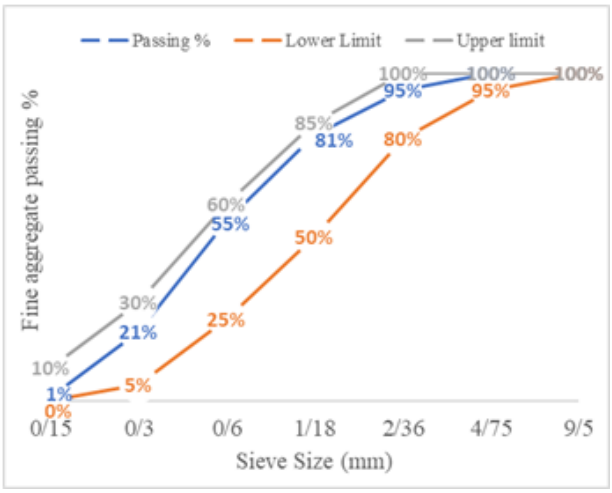

(a)

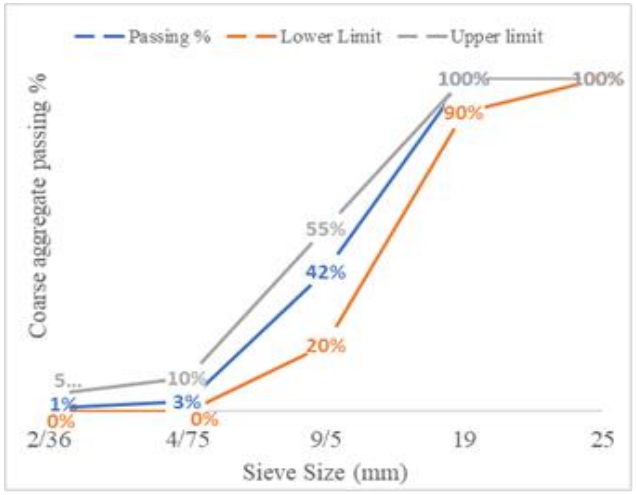

(b)

(c)

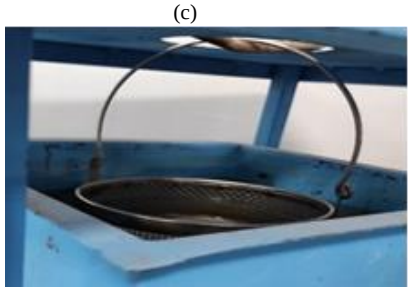

(d)

Figure 2. (a) Particle size distribution of sand, (b) particle size distribution of dolomite, (c) crushing test of dolomite, and (d) absorption test of dolomite.

Table 3.
Chemical composition of used cement (% mass)

SiO_2	CaO	Al_2O_3	Fe_2O_3	MgO	SO_3	Na_2O	P_2O_5	Cl	TiO_2	LOI*
21.52	61.89	3.8	1.88	2.26	2.81	0.55	0.21	0.14	0.51	3.11

* LOI: Loss on Ignition at 1000 ◦C.

Table 4.
Physical properties of the used aggregates.

Property	Specific gravity	Bulk density (kg/m3)	Voids (%)	Absorption (%)	Clay and fine materials (%)	Crushing Value (%)	Fineness modulus
Fine Aggregate	2.55	1745	31.6	0.8	1	--	2.47
Coarse Aggregate	2.68	1675	37.5	0.45	0.5	19	--

Table 5.
properties of the used superplasticizer.

Manufacturer's recommended ratio	Color	Raw material	Density	PH value	Solid content ratio	Category
1% to 3% of water weight	Dark Brown Liquid	Sulfonated Naphthalene Formaldehyde	1.2 kg/L	(8.5 ± 1)	30%	high-range water reducer derived from modified polycarboxylates

Table 6.
Chemical composition of RHA powder (% mass).

SiO_2	CaO	Al_2O_3	Fe_2O_3	MgO	K_2O	Na_2O	SO_3	P_2O_5	Cl	LOI
26.30	0.33	16.90	0.17	0.29	1.16	0.27	0.68	0.27	0.40	53.20

Table 7.
Mix design of the investigated RHA concrete mixes in (kg/m3).

Mix description	ID	Cement (kg)	Aggregate (kg)		Water (lit)	SP (kg)	RHA (kg)
			dolomite	sand			
Control mix	CO	380	1190	720	142.5	1.5	-
5% RHA	5RHA	361	1190	720	142.5	1.5	19
10% RHA	10RHA	342	1190	720	142.5	1.5	38
15% RHA	15RHA	323	1190	720	142.5	1.5	57
20% RHA	20RHA	304	1190	720	142.5	1.5	76
25% RHA	25RHA	285	1190	720	142.5	1.5	95

(a) (b)

Figure 3. (a) Mixing and curing water, and (b) the used SP (Sikament NN).

(a)

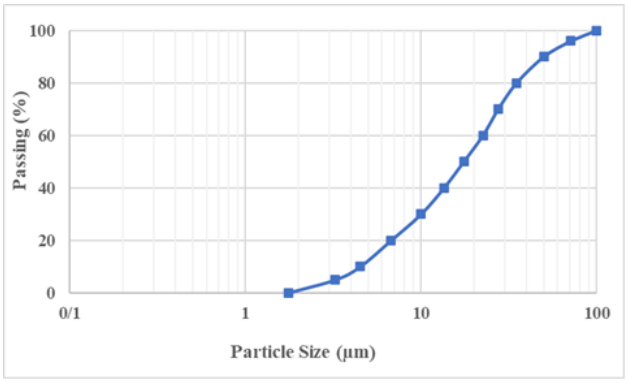

(b)

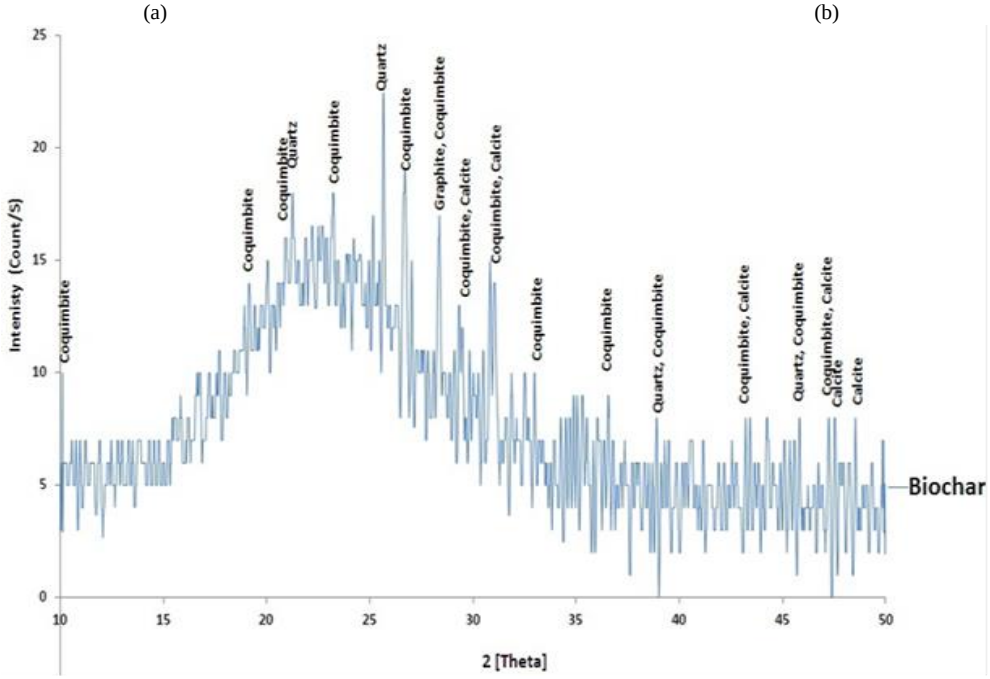

(c)

Figure 4. (a) Appearance of RHA powder after grinding, (b) Particles size distribution of RHA, and (c) XRD patterns of RHA powder.

Figure 5. Sample of RHA mortar and concrete cubes.

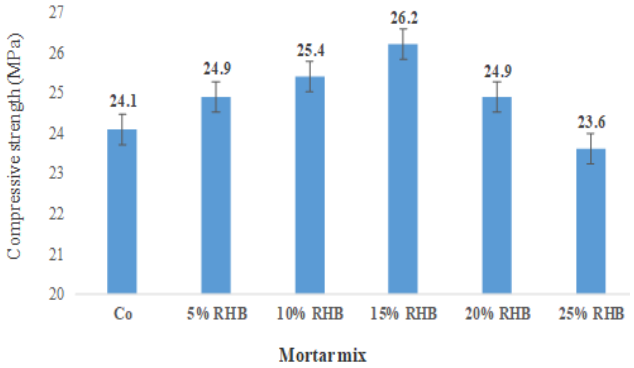

Figure 6. Compressive strength of mortar cubes

3.4.2. Mechanical properties

The compressive strength of the concrete mixtures incorporating different RHA replacement ratios was determined using standard cube specimens measuring 100 × 100 × 100 mm. For each mix, three specimens were tested, and the reported value represents the average compressive strength at 28 days of curing. The tests were conducted using a uniaxial compression testing machine with a capacity of 3000 kN.The same testing machine was also employed to determine the splitting tensile strength of cylindrical concrete specimens with dimensions of 100 mm in diameter and 200 mm in height, after 28 days of curing. The splitting tensile strength test was performed by applying a compressive load along the longitudinal axis of the cylinder until failure occurred. During testing, the cylinders were placed horizontally between the loading platens of the testing machine, and a continuous load was applied until the specimen fractured.

For each concrete mix, three cylindrical specimens were tested, and the reported splitting tensile strength values correspond to the average of the three results obtained under identical mix conditions

3.4.3. Microstructural analysis

Microstructural characterization of the concrete specimens was carried out using X ray Diffraction (XRD) and Energy Dispersive X ray Spectroscopy (EDX). XRD is a fundamental analytical technique for examining the mineralogical composition and hydration behavior of cement-based materials. It enables the identification of crystalline phases, which possess long range atomic order, as well as amorphous phases that lack such ordering. Owing to its capability to track phase evolution, XRD is widely used in concrete research to analyze cement, crushed concrete powder, hydrated cement paste, and supplementary cementitious materials such as pozzolans and nanomaterials.

In this study, RHA powder was first examined by XRD to validate its chemical composition and to confirm its predominantly amorphous silica structure, as suggested by complementary characterization methods. In addition, six powdered samples obtained from both the control and RHA modified concrete mixes were prepared by crushing the hardened concrete and sieving the resulting powder to pass a 75 µm sieve. These samples were subjected to XRD analysis to provide microstructural interpretation of the mechanical strength trends observed across different RHA replacement levels.

Elemental analysis was performed using EDX, which allows quantitative determination of elemental weight percentages within the concrete matrix. The EDX results served two essential purposes:Providing input data for the Monte Carlo and PhyX radiation shielding simulations described in Section 4. Evaluating compositional variations, particularly changes in the calcium to silicon (Ca/Si) ratio, which are known to influence hydration processes and the mechanical properties of cementitious systems.

3.4.4. Radiation shielding measurements

To assess the radiation shielding capabilities of the prepared concrete mixes, both simulation and computational approaches were employed. Monte Carlo simulations and Phy-X software were used to evaluate the radiation shielding performance against gamma and fast neutrons.

3.4.4.1. MC Simulation

In this work, the Monte Carlo method was used to simulate the movement of natural particles as well as to predict the gamma/neutron radiation performance., in the energy range of gamma rays (γp) at $0.015 \leq \gamma p \leq 15$ MeV. The goal is to determine and compare the intensity of γ-rays before and after passing through the samples under study. This code is used in the study of radiation shielding, as well as calculating radiation doses in addition to detector design [46]. The simulation code features operation across a wide range of energy levels, accommodating all different engineering designs and enabling rapid calculations. Several data lines must be available to create the input file for the code, which include the distance between the source and the detector, the dimensions of the source, the elemental composition, and the chemical composition of the samples under study. As shown in Figure 7, the geometric configuration for the simulation was created using a pre-set 3D setup. The data about the used code was detailed in the previous published work [47]. Also, the Phy-X/PSD (PhyX) was used to validate the MC results. It is an online tool for figuring out radiation doses and shielding characteristics [48-50].

The concrete shield consists of concrete cubes representing the control mix and the mixes containing increasing proportions of RHA, each with dimensions of 100 × 100 × 100 mm, where the shield thickness is 10 cm. This thickness is substituted into the Beer-Lambert equation as follows [51]:

$$\mu, \text{cm-1} = (1/T) \ln (C/C0) \quad (1)$$

where μ is the linear attenuation coefficient (cm^{-1}), T is the material thickness (cm), and C_0 and C are the initial and final counts of gamma-ray photons measured before and after shielding. Additionally, the values of other γ-ray attenuation parameters, such as the half-value thickness (HVT), tenth-value thickness (TVT), mean free path (MFP), effective atomic number (Zef), transfer factor (TF)

and radiation protection (RPE) were calculated using the following equations. [51-53]:

$$HVT, cm = \ln(2) / \mu \quad (2)$$

$$TVT, cm = \ln(10) / \mu \quad (3)$$

$$MFP, cm = 1 / \mu \quad (4)$$

Each of these attenuation parameters provides unique insights into the shielding performance of concrete against γ-rays. The mass attenuation coefficient represents the attenuation per unit mass and is crucial for comparing materials with different densities, making it a fundamental parameter in material selection for radiation shielding. The HVT and TVT are the thickness of material required to reduce the gamma-ray intensity by half and tenth, offering a practical measure of the material's efficiency in attenuating radiation. While HVT is often used for quick evaluations, TVT is more critical for scenarios requiring higher attenuation, highlighting the complementary nature of these parameters in assessing and optimizing shielding performance.

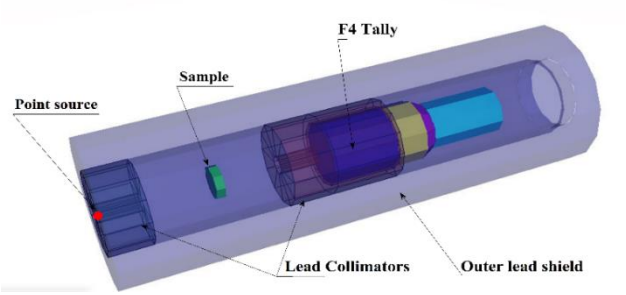

Figure 7. 3-D view of the radiation attenuation simulation system used for the prepared concrete samples

3.4.4.2. PhyX software

Phy-X is a web-based software tool designed for the assessment of radiation shielding parameters and radiation doses. It facilitates the determination of parameters including LAC, MAC, HVL, TVL, MFP, effective atomic number, and electronic density. These calculations are essential for the design of radiation protection materials used in X-ray and gamma-ray applications. The user-friendly interface allows input of the chemical composition of a given substance, enabling the computation of its properties across a broad spectrum of radiation energies and sources.

4. Experimental results

4.1. Physical properties results

4.1.1. Setting times and consistency results

Cement paste samples incorporating RHA exhibited higher standard consistency values compared with the control mix. This behavior can be attributed to several factors. First, the porous structure of RHA particles enables them to absorb and retain a considerable amount of water, thereby increasing the water demand required to achieve normal consistency during cement hydration.

Additionally, the chemical composition of the RHA used in this study (Table 6) contains a high proportion of silicon and aluminum oxides, accounting for 43.2% of the total mass and approximately 92.37% of the mineral fraction of the ash, excluding carbon content. Such a composition enhances the pozzolanic reactivity of RHA, which contributes to increased water consumption during the activation of hydration and pozzolanic reactions within the cementitious system.

Moreover, increasing the replacement ratio of cement with RHA further intensified this effect. The highest increase in standard consistency reached 35.7% at a replacement level of 25%, indicating a substantial rise in water demand as the RHA content increased.

Regarding the setting time of cement paste, a reduction in both initial and final setting times was observed for mixtures containing RHA up to a 15% replacement level. This trend supports the assumption that the RHA used in this study exhibits significant pozzolanic activity, which accelerates the early hydration reactions. Similar observations have been reported in several previous studies.[54-56], which attributed the reduction in initial and final setting times upon biochar addition to its filler effect and absorption of free water. The shortened setting time is attributed to biochar particles acting as filler and moisture absorbers. This effect is further influenced by the hydrophilic or hydrophobic nature of the biochar, which depends on its production temperature and contributes to micro-filling [57]. However, when the replacement ratio exceeded this threshold, an increase in setting times was observed. The recorded increases were slight, with the maximum increase in final setting time in the 25 RHA mix reaching 7.14% compared to the control mix. These results provide a preliminary indication that the optimal replacement ratios for the type of biochar powder used in the current study range from 10% to 15% of the cement weight. Figure 8 shows the values of setting times and consistency values of all designed mixes in this study.

4.1.2. Slump test result

The effect of using RHA powder as a partial cement replacement material on slump values was investigated. As shown in Figure 9, a significant decrease in slump values was observed. The porous microstructure and surface fineness of the RHA powder likely contributed to this reduction in slump, consequently affecting the workability of the resulting concrete. Biochar particles have been shown to retain higher amounts of free water within their

porous structure [54]. Replacing 25% of the cement with RHA resulted in a 57.3% decrease in slump values compared to the control mix.

These findings align with previous research on other biochar types, which indicates that increasing the proportion of biochar in concrete mixes generally leads to decreased workability [58].

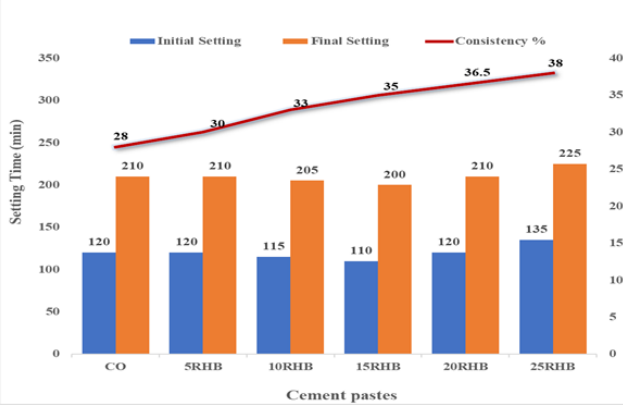

Figure 8. Setting times and consistency values of control and RHA cement pastes

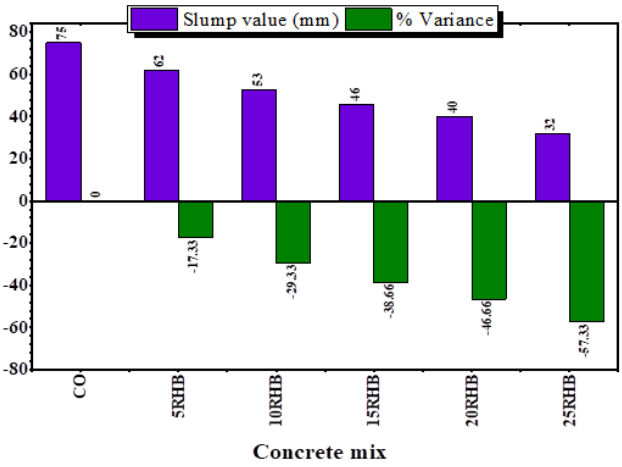

Figure 9. Slump values for control and RHA concrete mixes.

4.2. Mechanical properties results

4.2.1. Compressive strength results

The compressive strength results of the control and RHA modified concrete specimens, presented in Figure 10, demonstrate the potential of rice husk ash (RHA) to enhance the compressive strength of concrete. The improvement in mechanical performance can be attributed primarily to the chemical composition and moderate pozzolanic activity of RHA. This interaction promotes the formation of additional calcium silicate hydrate (C–S–H) gel, which is the main strength giving phase in cementitious systems.

Moreover, the fine particle size of RHA contributes to a filler effect, allowing the particles to occupy micro voids within the cement matrix. This process increases the overall density of the concrete and refines the pore structure by reducing pore size and connectivity. As a result, the microstructure becomes more compact, which enhances the mechanical performance of the concrete.

Among the mixtures containing RHA, the 10% replacement level of cement with RHA provided the most favorable result, producing a 13.74% increase in compressive strength compared with the control mixture. This optimal replacement ratio is consistent with the findings reported by Gomes et al., who also observed improved compressive strength at moderate RHA substitution levels. [59], who reported that incorporating 5% and 10% water treatment sludge biochar enhanced the compressive strength of natural sludge mortar by 37% and 46%, respectively. Other studies have also demonstrated optimal concrete performance at a 10% biochar replacement ratio, albeit with varying degrees of improvement [29, 30]. The biochar used in this study is characterized by a higher combined percentage of silicon and aluminum oxides (43.2%) compared to other biochar types previously incorporated into concrete. For example, rice husk ash used by Yang et al. (2021) [60] In contrast, the RHA used in the study by Gomes et al. contained only 16.51% of the key oxides responsible for enhancing pozzolanic reactions. This relatively low content of reactive silica and alumina, combined with the high porosity of the biochar particles, resulted in a 5.5% reduction in compressive strength at a 5% cement replacement level after 28 days of curing.

In the present study, however, even a 25% replacement ratio produced compressive strength values comparable to the control mix, underscoring the potential for incorporating relatively high amounts of this biochar into concrete without compromising mechanical performance. This finding highlights a promising avenue for developing more sustainable and environmentally friendly concrete.

The sustainability benefits arise from the fact that biochar acts as a stable carbon-rich material derived from organic feedstocks that would otherwise decompose or combust, releasing CO_2 into the atmosphere. When incorporated into concrete, the biochar's stable carbon structure remains locked within the matrix, enabling long-term carbon sequestration and significantly reducing the concrete's overall carbon footprint.

4.2.2. Tensile strength results

The highest splitting tensile strength of the concrete cylinders was achieved at a 15% replacement level of RHA, as shown in Figure 11. At this optimal dosage, the tensile strength exhibited a 9.48% increase compared with

the control mix. Beyond the 15% replacement level, a marginal decline in tensile strength was observed; however, all RHA containing mixes continued to outperform the control sample. Notably, even the highest replacement ratio of 25% RHA maintained tensile strength values comparable to the control, with a slight improvement of approximately 1.83%. These results reinforce the feasibility of using RHA as a high volume cement replacement while preserving acceptable mechanical performance.

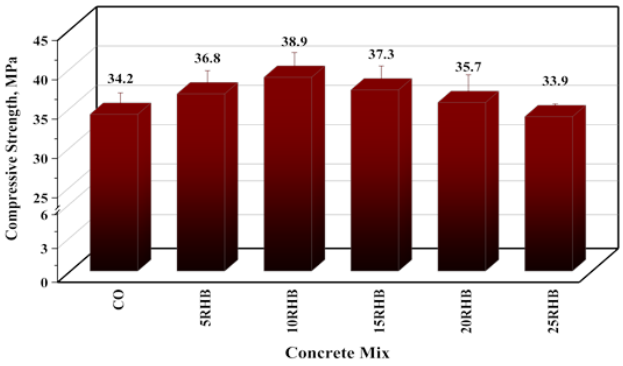

Figure 10. Compressive strength for control and RHA concrete specimens.

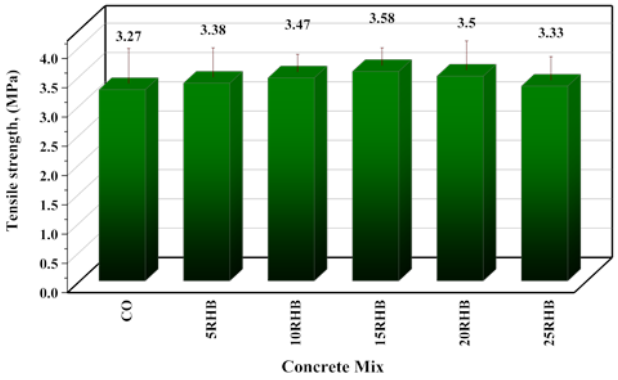

Figure 11. Tensile strength for control and RHA concrete specimens.

In addition to the mechanical advantages, the incorporation of RHA offers substantial environmental benefits, including reduced CO_2 emissions associated with cement manufacturing, diversion of agricultural waste from disposal, and enhanced sustainability of concrete materials.

The mechanical behavior observed in this study highlights a nuanced response of concrete to RHA incorporation. While the 10% replacement level yielded the highest compressive strength—likely due to moderate pozzolanic activity, increased C–S–H gel formation, and microstructural densification through the filler effect—the peak tensile strength at 15% RHA suggests that different mechanisms govern tensile resistance. At higher RHA contents, the distinctive characteristics of the biochar, such as its fibrous morphology and internal porosity, appear to contribute positively to tensile performance. These features may provide crack bridging capabilities, where fibrous RHA particles span developing microcracks under tensile loading, thereby delaying crack propagation. Additionally, the porous structure of RHA can facilitate stress redistribution, reducing local stress concentrations and enhancing the tensile load carrying capacity of the concrete matrix.

4.3. Microstructural analysis results

4.3.1. XRD analysis

X ray diffraction (XRD) is a fundamental technique for investigating the complex hydration processes of cementitious materials. By providing detailed information on mineralogical composition and phase evolution, XRD offers valuable insight into the mechanisms governing the development and performance of cement paste. In this study, XRD analysis was performed to investigate the composition and hydration products of cement pastes containing different proportions of rice husk ash (RHA).

Six cement paste samples were analyzed after 28 days of moisture curing, including the control mix (CO) and mixes containing 5%, 10%, 15%, 20%, and 25% RHA (5RHA, 10RHA, 15RHA, 20RHA, and 25RHA), as illustrated in Figure 12. The XRD patterns revealed the presence of calcium silicate hydrate (C–S–H, PDF#00 033 0306) and portlandite (CH, PDF#00 004 0733) as the primary hydration products in all samples, confirming their well established roles in cement hydration and strength development. In addition, minor peaks corresponding to ettringite (PDF#00 041 1451) and quartz (SiO_2 , PDF#01 083 0539) were detected.

Among these phases, C–S–H is the most critical compound governing the mechanical performance of concrete, as it forms directly during cement hydration and acts as the primary binding phase within the cement matrix. A higher content of C–S–H contributes to the formation of a denser and stronger interfacial transition zone (ITZ) between the cement paste and aggregates, thereby enhancing the overall mechanical properties of concrete, particularly its compressive strength.

The presence of portlandite (CH) plays a more complex role in concrete performance. At moderate levels, portlandite can contribute to reducing pore volume and may slightly enhance strength due to its crystalline structure. However, excessive or insufficient quantities of portlandite can adversely affect both strength and durability, as high CH content may increase vulnerability to chemical attack, while reduced CH availability may limit the progression of hydration reactions.

[61]. The presence of quartz (silica) particles helps in more densification of the concrete matrix and formation of CSH gel. It is also responsible for enhancing the ITZ

between the aggregate and cement paste matrix. Ettringite plays a complex role in concrete. While controlled formation can contribute to a denser microstructure and improved properties, excessive formation can have detrimental effects [62].

Figure 12 demonstrates an increase in CSH peak intensity in RHA samples compared to the control mix, with the most pronounced peaks observed at 10% and 15% RHA incorporation. This increase coincides with a slight reduction in portlandite peaks, suggesting moderate pozzolanic activity of the RHA. The significant increase in CSH intensity observed in the 10% and 15% RHA pastes compared to the control highlights the influence of RHA on the hydration process. RHA's porous structure and functional groups can interact with cement components, potentially influencing hydration kinetics and the formation of hydration products. The high silicon and aluminum oxide content (approximately 43%) of the biochar used in this study suggests moderate pozzolanic potential. Furthermore, RHA incorporation can enhance concrete durability by reducing permeability, improving chloride ion resistance, and refining the overall microstructure, as reported in the literature [63]. XRD analysis provided further insights into the mineralogical transformations within the concrete matrix. While ettringite peaks were evident in both control and RHA samples, a slight reduction in their intensity was observed in the RHA samples, likely attributed to the consumption of calcium ions by pozzolanic reactions between the RHA and the cement. Conversely, the presence of quartz peaks, originating from the silica content within the RHA, was evident and their intensities generally increased with increasing RHA percentages.

This observation, coupled with the enhanced CSH formation and the observed reduction in portlandite, indicates that the incorporation of RHA significantly alters the mineralogical composition of the concrete matrix. These findings provide valuable insights into the mechanisms underlying the observed improvements in the mechanical properties of the RHA-modified concrete.

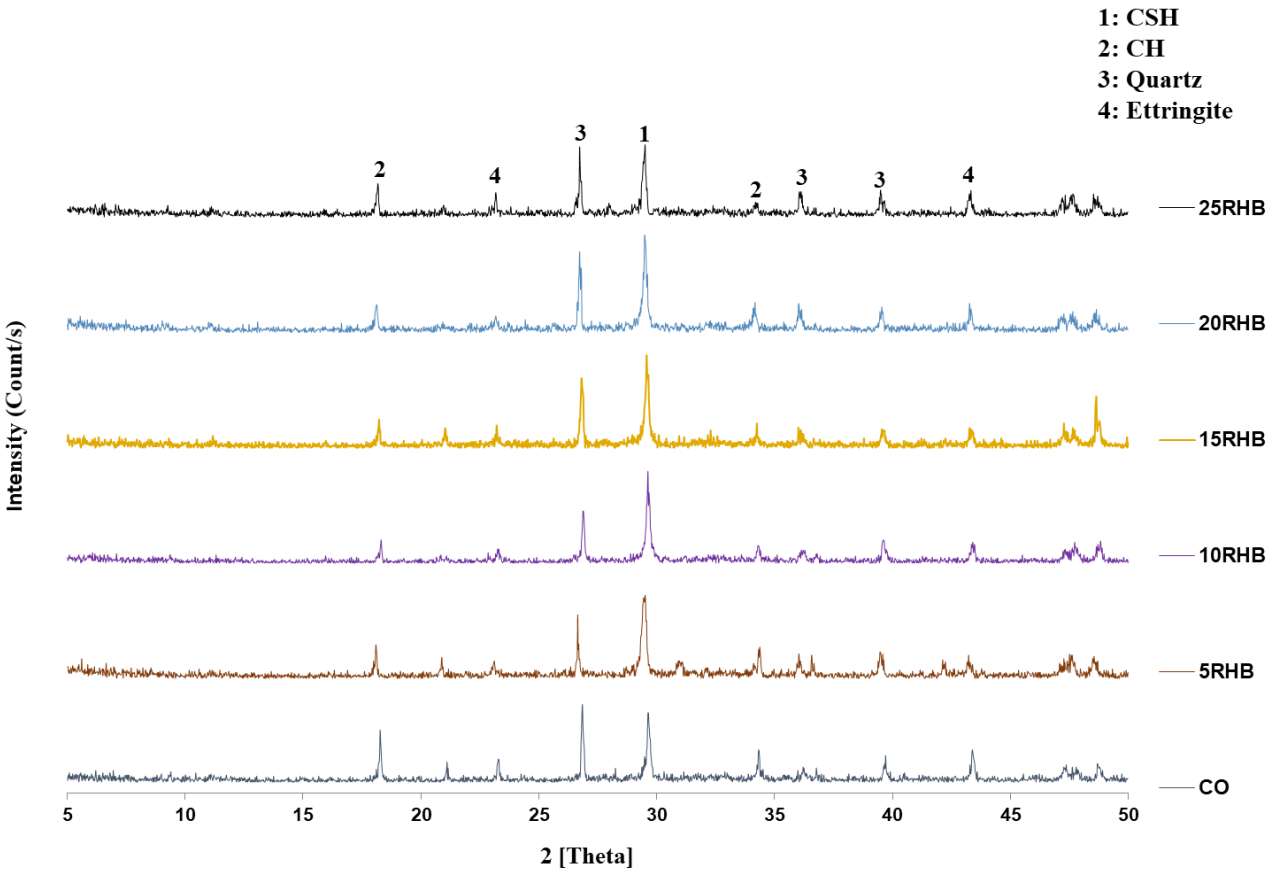

Figure 12. XRD patterns of the control and RHA mixes.

4.3.2. EDX analysis results

As previously discussed, energy dispersive X ray spectroscopy (EDX) was employed to chemically characterize the concrete samples and determine the elemental weight percentages of their constituents. This analysis enabled a comparative evaluation of the elemental composition of the different mixtures. The obtained results served two main purposes. First, they provided the necessary input data for developing radiation shielding simulation models using Monte Carlo (MC) codes and the Phy X software, as described in Section 5. Second, they were used to interpret variations in mechanical strength by examining key compositional parameters, particularly the Ca/Si ratio.

An increase in carbon content was observed in concrete mixtures with higher RHA replacement levels. This increase can be attributed to the fact that more than 52% of the RHA composition consisted of carbon, which was volatilized during the XRF analysis used to determine the chemical composition of RHA.

The Ca/Si ratio was identified as a critical parameter influencing the strength development of the concrete mixtures. Adjusting this ratio through the appropriate selection and proportioning of cementitious materials and admixtures allows the properties of concrete to be optimized for specific performance requirements, thereby improving both structural efficiency and durability.

A clear trend was observed in which a reduction in the Ca/Si ratio corresponded to increased polymerization of the C–S–H gel, resulting in enhanced compressive strength. Within the hardened cement matrix, the Ca/Si ratio of the C–S–H phase serves as an indicator of the degree of polymerization of hydration products. Lower Ca/Si ratios generally indicate a higher degree of polymerization, reflecting the formation of longer and more interconnected C–S–H chains, which contribute to improved mechanical performance. These findings are consistent with the results reported by Kim (2013).[63], a reduction in the Ca/Si ratio within the C-S-H phase is associated with C-S-H chain elongation and increased polymerization. In agreement with Choudhary et al. (2021) [64] and Dadsetan and Bai (2017) [65], a strong correlation was observed between compressive strength and the Ca/Si ratio: a decrease in the Ca/Si ratio corresponded to an increase in compressive strength. These findings emphasize the critical role of C-S-H polymerization in enhancing concrete's mechanical properties. Several literature studies [66, 67] also demonstrated a clear inverse relationship between the Ca/Si ratio and concrete compressive strength. Figure 13 presents EDX patterns of the primary elements that constitute the hydration products in different concrete specimens, which include O, Ca and Si peaks as detailed by (wt.%) in Table 8. Notably, Figure 13 also includes C peak, enabling a comparative analysis of carbon levels between RHA samples and the control. Figure 13 illustrates the comparison between EDX spectra for concrete specimens. Table 8 provides the EDX results for the different mixes and shows the Ca/Si ratio, which is an indicator for C-S-H in concrete which plays an important role in strength development of concrete as previously mentioned. The results show that the Ca/Si ratios of 5.95, 5.69, 4.84, 4.89, 5.11, and 5.6 for CO, 5RHA, 10RHA, 15RHA, 20RHA, and 25RHA, respectively. From the results, it can be concluded that the order in Ca/Si ratio is CO > 5RHA > 25RHA > 20RHA > 15RHA > 10RHA. EDX analysis revealed a correlation between Ca/Si ratio and mechanical properties, with lower Ca/Si ratios generally resulting in higher compressive strengths. While the order of Ca/Si ratios did not perfectly align with the order of compressive strengths, the correlation was strong. Notably, the 10% RHA sample, exhibiting the lowest Ca/Si ratio, demonstrated the highest compressive strength, supporting the observed trend.

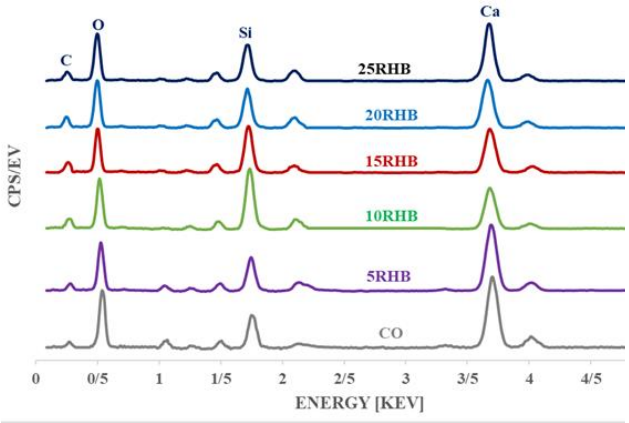

Figure 3. Decomposition of $M_b^{\infty}(t)$

Table 8.
EDX results for different concrete mixes.

Element	Composition (wt.%)					
	CO	5RH	10RH	15RH	20RH	25RH
O K	38.1	39.01	40.9	41.11	39.85	38.46
Ca K	41.3	38.92	34.99	35.11	35.91	37.25
Si K	6.95	6.84	7.23	7.18	7.03	6.65
Al K	1.46	1.47	1.72	1.46	1.31	1.22
Fe K	1.68	1.53	1.63	1.46	1.25	1.23
Mg K	0.33	0.29	0.31	0.33	0.3	0.25
Na K	1.97	1.66	1.79	1.37	1.15	1.17
C K	8.11	10.27	11.43	11.97	13.19	13.75
Density	2.45	2.52	2.57	2.6	2.58	2.55
Ca/Si	5.95	5.69	4.84	4.89	5.11	5.6

5. Radiation shielding performance

5.1. Gamma attenuation

The LAC by MCNP and Phy-X in the photon energy (γp) range of 0.015–15 MeV is shown in Table 9. With a maximum Δ of 2.814%, the values of simulated LAC were in decent agreement with the values determined by Phy-X. The LAC value of the X-RHA concrete samples under investigation decreases as the γ-energy rises. For X-RHA concrete samples, the simulated LAC values decline as follows: 38.657 to 0.057 cm-1 for CO sample, 35.675 to 0.058 cm-1 for 5RHA sample, 33.815 to 0.058 cm-1 for 10RHA sample, 33.960 to 0.058 cm-1 for 15RHA sample, 33.625 to 0.058 cm-1 for 20RHA sample, and 33.390 to 0.057 cm-1 25RHA sample at γp range from 0.015 to 15 MeV. Figure 14(a) shows an abrupt decrease in LAC for each of the X-RHA concrete samples under study because of the PEE interaction, which has changed the cross-section (σp) with γ -3: 5 [68-70]. We observe that when the values of γp energy increase from 0.015 to 0.2 MeV, σp decreases significantly, and the PEE interaction consequently decreases. For X-RHA concrete samples, there is a strong tendency to decrease from 38.657 to 0.311 cm-1 for CO sample, 35.675 to 0.319 cm-1 for 5RHA sample, 33.815 to 0.324 cm-1 for 10RHA sample, 33.960 to 0.328 cm-1 for 15RHA sample, 33.625 to 0.325 cm-1 for 20RHA sample, and 33.390 to 0.322 cm-1 for 25RHA sample.The expected LAC in the γp range from 0.300 to 15 MeV decreases exponentially when γp from 0.300 to 15 MeV is increased, as shown in Figures 14(b,c). The CM interaction and the σp changes brought on by γp-1 are responsible for the exponential decline [71]. This effect can be explained by the fact that because of its increased speed, a larger γp has a lower tendency to interact with the atoms of the material. Consequently, the probability of γp interaction decreases, and the likelihood of γp scattering increases as the energy level rises. A smooth decline in LAC values followed a gradual decrease in σp with fewer electron-γp interactions, which was linked to an increase in γp values. So, the LAC values gradually decrease from 0.262 to 0.57 cm-1 for the CO sample, 0.269 to 0.058 cm-1 for the 5RHA sample, 0.274 to 0.058 cm-1 for the 10RHA sample, 0.278 to 0.058 cm-1 for 15RHA sample, 0.276 to 0.058 cm-1 for 20RHA sample, and 0.273 to 0.057 cm-1 for 25RHA sample. We noted that the 15RHA sample has the highest LAC because of its high density, On the contrary, the 25RHA sample is a less valuable sample. The LAC for the mixed concrete samples and previously published doped concrete samples are compared in Figure 15. The samples of this study achieved results equal to those of the previously studied and published samples at 10 MeV, 0.5 MeV, and 5 MeV. It presents a comparison of the UHPC samples with commercial concrete (mixes of PbO bulk powder with cement, with substitution ratios ranging from 1 to 5% %. Additionally, five other mixtures of GD bulk powder with cement increased the substitution rates to 9% and one hybrid mix combining 5% PbO and 7% GD [52]), Bashtar concretes (S-magnetite, S-scrap, ilmenite, H-serpentine, I-limonite, and B-magnetite [72]), and marble (MD) and granite (GD) waste dust of cement at a replacement ratio of 6%. Furthermore, two additional mixes with the cement weight of nano-alumina (NAl) [51]. The prepared concrete mix containing 15%BPA (15RHA) were higher than those compared (Bashtar concretes, 1BL, NA1, and (1-5) BG) at 0.5 and 10 MeV. Also, it higher than 1BL, 2BL, 1-9BG, MD6%, GD6%, NA1, and GD6%+NA1) at 5 MeV.

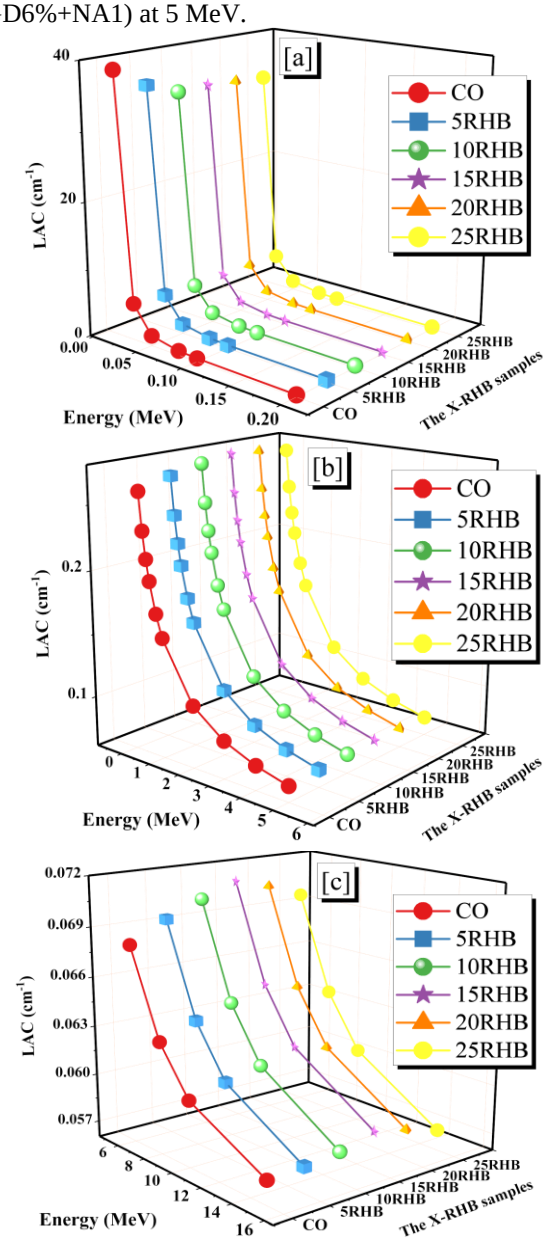

Figure 15. The linear attenuation (a) in the PEE region, (b and c) in the Compton region for the X-RHA concrete samples.

Table 9.
The linear attenuation (LAC), obtained using MCNP code and PhyX software for the prepared X-RHA Concrete samples.

Energy, (MeV)	The linear attenuation (LAC, cm^{-1})								
	CO			5RHA			10RHA		
	PhyX	MC	φ. (%)	PhyX	MC	φ. (%)	PhyX	MC	φ. (%)
0.015	38.745	38.657	0.225	35.754	35.675	0.222	33.887	33.815	0.213
0.03	5.467	5.445	0.408	5.080	5.060	0.404	4.840	4.822	0.388
0.05	1.512	1.492	1.339	1.437	1.418	1.326	1.391	1.373	1.273
0.08	0.653	0.636	2.655	0.643	0.626	2.629	0.637	0.621	2.526
0.1	0.505	0.490	2.814	0.504	0.490	2.787	0.505	0.491	2.677
0.2	0.319	0.311	2.444	0.326	0.319	2.420	0.331	0.324	2.325
0.3	0.267	0.262	1.712	0.274	0.269	1.695	0.279	0.274	1.628
0.4	0.236	0.233	1.289	0.243	0.240	1.277	0.247	0.244	1.226
0.5	0.215	0.212	1.059	0.221	0.218	1.049	0.225	0.223	1.007
0.6	0.198	0.196	0.958	0.204	0.202	0.948	0.208	0.206	0.910
0.8	0.174	0.172	0.725	0.179	0.177	0.717	0.182	0.181	0.689
1	0.156	0.155	0.694	0.160	0.159	0.688	0.163	0.162	0.660
2	0.110	0.109	0.580	0.113	0.112	0.574	0.115	0.114	0.551
3	0.090	0.090	0.482	0.092	0.092	0.477	0.094	0.094	0.458
4	0.079	0.079	0.304	0.081	0.081	0.301	0.082	0.082	0.289
5	0.073	0.072	0.279	0.074	0.074	0.277	0.075	0.075	0.266
6	0.068	0.068	0.255	0.069	0.069	0.252	0.070	0.070	0.242
8	0.063	0.063	0.225	0.064	0.064	0.223	0.064	0.064	0.214
10	0.060	0.060	0.295	0.061	0.061	0.292	0.061	0.061	0.281
15	0.058	0.057	0.092	0.058	0.058	0.092	0.058	0.058	0.088

Energy, (MeV)	The linear attenuation (LAC, cm^{-1})								
	CO			5RHA			10RHA		
	PhyX	MC	φ. (%)	PhyX	MC	φ. (%)	PhyX	MC	φ. (%)
0.015	38.745	38.657	0.225	35.754	35.675	0.222	33.887	33.815	0.213
0.03	5.467	5.445	0.408	5.080	5.060	0.404	4.840	4.822	0.388
0.05	1.512	1.492	1.339	1.437	1.418	1.326	1.391	1.373	1.273
0.08	0.653	0.636	2.655	0.643	0.626	2.629	0.637	0.621	2.526
0.1	0.505	0.490	2.814	0.504	0.490	2.787	0.505	0.491	2.677
0.2	0.319	0.311	2.444	0.326	0.319	2.420	0.331	0.324	2.325
0.3	0.267	0.262	1.712	0.274	0.269	1.695	0.279	0.274	1.628
0.4	0.236	0.233	1.289	0.243	0.240	1.277	0.247	0.244	1.226
0.5	0.215	0.212	1.059	0.221	0.218	1.049	0.225	0.223	1.007
0.6	0.198	0.196	0.958	0.204	0.202	0.948	0.208	0.206	0.910
0.8	0.174	0.172	0.725	0.179	0.177	0.717	0.182	0.181	0.689
1	0.156	0.155	0.694	0.160	0.159	0.688	0.163	0.162	0.660
2	0.110	0.109	0.580	0.113	0.112	0.574	0.115	0.114	0.551
3	0.090	0.090	0.482	0.092	0.092	0.477	0.094	0.094	0.458
4	0.079	0.079	0.304	0.081	0.081	0.301	0.082	0.082	0.289
5	0.073	0.072	0.279	0.074	0.074	0.277	0.075	0.075	0.266
6	0.068	0.068	0.255	0.069	0.069	0.252	0.070	0.070	0.242
8	0.063	0.063	0.225	0.064	0.064	0.223	0.064	0.064	0.214
10	0.060	0.060	0.295	0.061	0.061	0.292	0.061	0.061	0.281
15	0.058	0.057	0.092	0.058	0.058	0.092	0.058	0.058	0.088

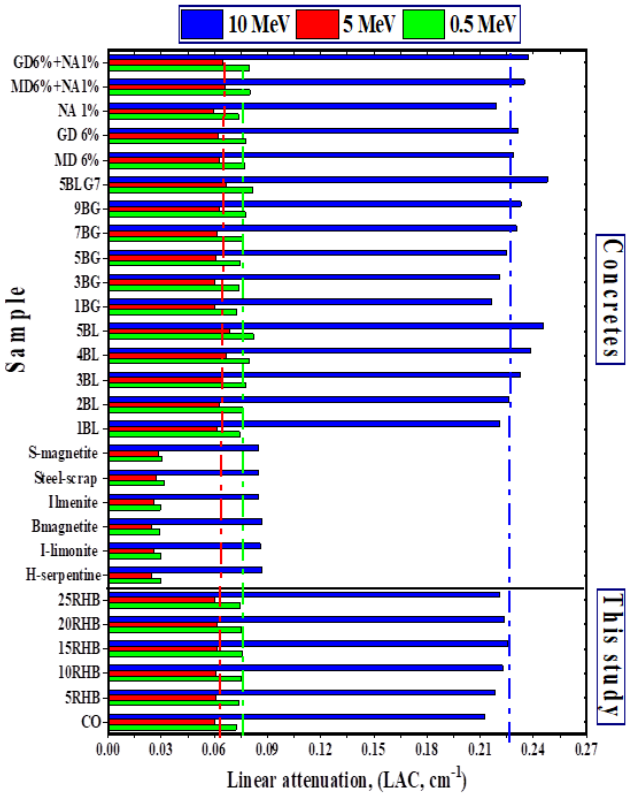

Figure 15. Comparison between the LAC for the mixed concrete samples with two previously published doped concrete samples.

The effectiveness of gamma ray shielding materials is commonly evaluated using three key parameters: the half value thickness (HVT), the tenth value thickness (TVT), and the mean free path (MFP). These parameters collectively describe both the required material thickness and the radiation attenuation capability. For a given photon energy, lower HVT, TVT, or MFP values indicate superior radiation shielding performance, as radiation is attenuated over a shorter distance.

The HVT and TVT values exhibit an inverse relationship with the linear attenuation coefficient (LAC). As the LAC decreases, both HVT and TVT increase. Over the photon energy range of 0.015–15 MeV, the HVT values increased from 0.018 to 12.061 cm for the CO sample, 0.019 to 12.036 cm for 5RHA, 0.020 to 11.991 cm for 10RHA, 0.020 to 11.870 cm for 15RHA, 0.021 to 11.974 cm for 20RHA, and 0.021 to 12.106 cm for 25RHA. As shown in Figure 16(a), the 15RHA sample exhibited the lowest HVT values due to its highest LAC, whereas the 25RHA sample displayed the highest HVT values, corresponding to its lower LAC.

A similar trend was observed for the TVT values, as illustrated in Figure 16(b). The TVT increased from 0.060 to 40.066 cm for the CO mix, 0.065 to 39.984 cm for 5RHA, 0.068 to 39.432 cm for 10RHA, 0.068 to 39.778 cm for 15RHA, 0.068 to 39.778 cm for 20RHA, and reached its highest values for the 25RHA mix. Consistent with HVT behavior, the 25RHA sample exhibited the highest TVT values due to its low LAC, while the 15RHA sample showed the lowest TVT values, confirming its superior gamma ray attenuation capability.

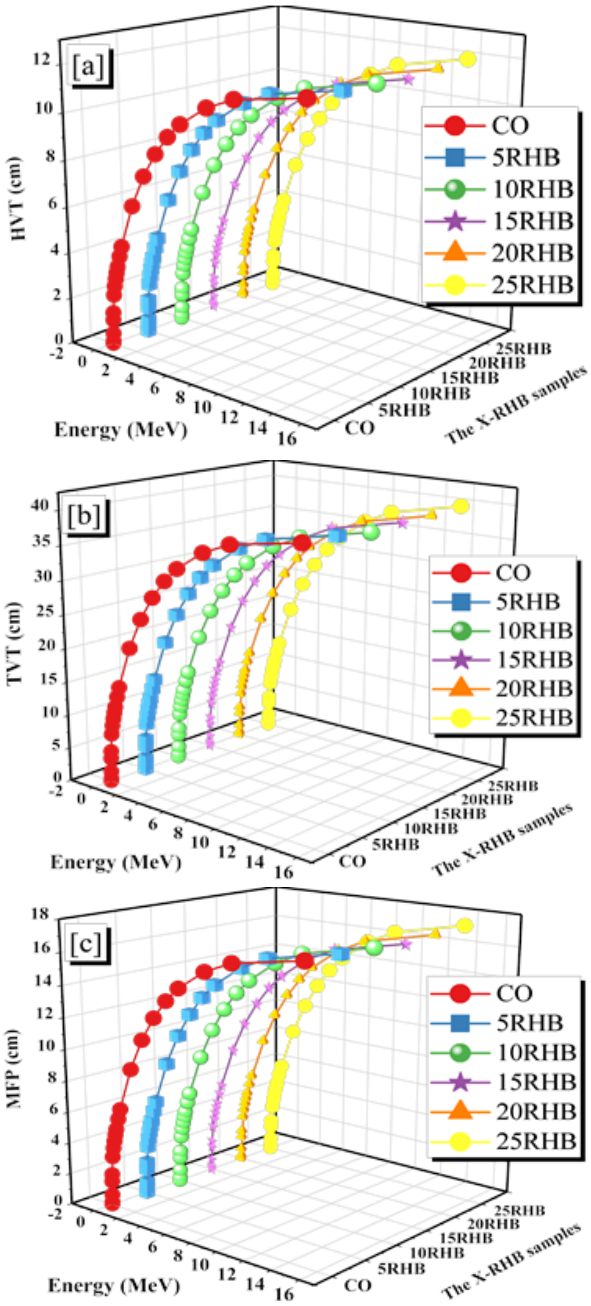

Figure 16. displays the concrete samples' HVT, TVT, and MFP in relation to γ-energy.

The mean free path (MFP) provides additional insight into how effectively a material absorbs or scatters gamma radiation. A lower MFP indicates a higher probability of photon interaction within a shorter distance, reflecting improved shielding efficiency. Consequently, evaluating

the MFP is critical when selecting and designing materials for radiation shielding applications in nuclear, medical, and industrial environments, where effective protection of personnel and equipment is essential. [73]. From 0.026 to 17.400 cm for CO, from 0.028 to 17.365 cm for 5RHA, from 0.030 to 17.300 cm for 10RHA, from 0.029 to 17.125 cm for 15RHA, from 0.030 to 17.275 cm for 20RHA, and from 0.030 to 17.466 cm for 25RHA, the MFP values for the X-RHA concrete samples increase as γp energies increase from 0.015 to 15 MeV. MFP values are lowest in the 15RHA sample and highest in the 25RHA sample as shown in Figure 16(c) and that is due to the inverse relationship between MFP and LAC [74].

For the X-RHA concrete samples, Figure 17 displays graphs of the adequate atomic number versus γ-energy ranging from 0.015 to 15 MeV. A higher Zef value indicates a greater interaction with radiation through mechanisms like PEE/Compton interactions. Materials with a higher Zef value may be better for protecting against high-energy [75]. As the γp rises for the materials under study, the Zef values fall. The concrete's Zef ranged from 18.407 to 12.525 for CO, 18.078 to 11.751 for 5RHA, 17.833 to 11.358 for 10RHA, 17.806 to 11.298 for 15RHA, 17.806 to 11.241 for 20RHA, and 17.821 to 11.251 for 25RHA concrete sample, depending on the energy spectra specified in this study. Given this, it is feasible to conclude that the radiation shielding efficiency of materials varies with the radiation energy; that is, certain substances may be more effective at higher or lower energies than others. Due to its content of elements with a high atomic number and its high density compared to the other samples in this study, the 15RHA sample had the highest value of Zef.

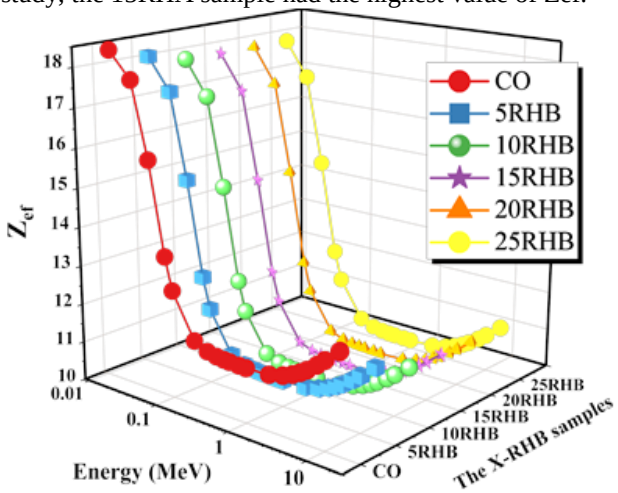

Figure 17. The Zef for the concrete samples as a function of photon energy.

5.2. Neutron attenuation

The radiation scattering ability of biochar has been explored in a limited number of studies [76, 77], Previous studies have reported that incorporating biochar into concrete can significantly enhance neutron shielding performance, particularly as the biochar content increases. This improvement is primarily due to the high carbon content of biochar. Carbon interacts strongly with neutrons through elastic scattering mechanisms, and these interactions depend on factors such as neutron energy, carbon isotope composition, and scattering angle. As a result, carbon rich composites often exhibit superior neutron attenuation compared with their γ radiation shielding performance. Carbon's neutron scattering characteristics make it an essential element for radiation protection materials used in nuclear reactors, shielding systems, and neutron related experimental research. Despite these promising findings, further studies are still required to fully understand the neutron shielding mechanisms in biochar based concretes.

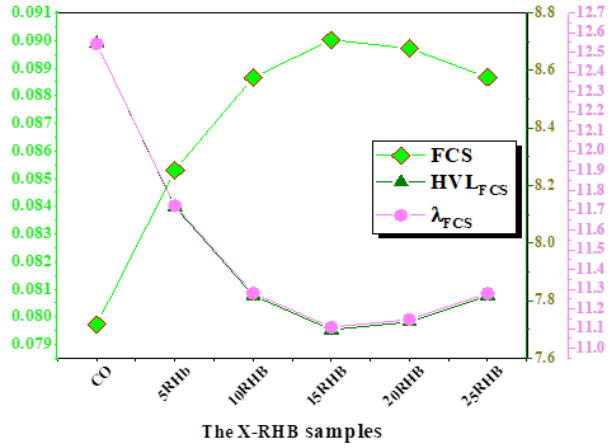

(a)

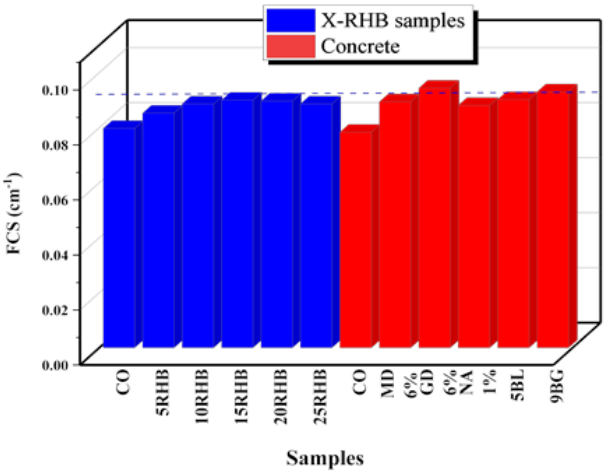

(b)

Figure 18. (a) The mixed concrete's fast neutron removal cross-section (FCS), half value layer (HVLFCS), and relaxation length (λFCS); (b) Comparison of the fast neutron removal cross-section (FCS) for the prepared X-RHA samples and previously published glass and concrete samples.

In this study, the fast neutron removal cross section (FCS), half value layer based on FCS (HVLFCS), and mean free path based on FCS (λFCS) for the RHA modified concrete samples are presented in Figure 18(a). Among all mixtures, the 15RHA sample demonstrated the highest FCS value of 0.090 cm^{-1}, along with the lowest HVLFCS (7.699 cm) and lowest λFCS (11.107 cm). These results indicate that the 15RHA mixture exhibits the strongest neutron shielding capability. This enhanced performance can be attributed to its relatively higher density and increased concentration of light elements, particularly carbon and oxygen, which are highly effective in moderating and scattering fast neutrons.

Figure 18(b) provides a comparative assessment between the concrete samples tested in this study and previously published concrete composites, further highlighting the competitive neutron shielding performance of the RHA based formulations.

[51, 52, 72] . From this comparison, it is clear that the RHA samples were higher than most of the compared concretes. The 15RHA sample was found higher than those compared except GD6% and 9BG samples.

6. Conclusions and future studies

This study examined the use rice husk ash, RHA as a partial cement replacement in concrete at substitution levels up to 25%. The biochar employed—distinguished by its unique chemical composition—represents an environmentally sustainable alternative to traditional cement. By reducing cement consumption, which is responsible for high energy demand and significant CO_2 emissions, RHA serves as a carbon sequestration medium. Its stable structure effectively immobilizes carbon within the matrix, contributing to greenhouse gas mitigation. Formulated with high proportions of silicon and aluminum oxides to promote pozzolanic activity, the material enhanced the concrete's physical, mechanical, and microstructural performance. In addition, the influence of different RHA replacement levels on radiation shielding capability was assessed using simulation codes for both γ ray and neutron radiation.

1- The incorporation of rice husk ash (RHA) had only a marginal influence on the setting times of the concrete mixes. Final setting time decreased slightly—by 4.76% relative to the control—at replacement levels up to 15%. However, beyond this threshold, a minor increase in final setting time was observed, reaching a maximum rise of 7.14% compared with the control mix at a 25% replacement level.

2- The incorporation of RHA had a more pronounced impact on standard consistency. As the RHA replacement level increased, the water demand required to achieve standard consistency also rose steadily, reaching a maximum increase of 35.7% at the 25% replacement level compared with the control mix. This increase in water demand is attributed to the porous structure of the biochar, which elevates its water absorption capacity, as well as its high specific surface area, which necessitates additional water to adequately wet the particles and achieve the required workability.

3. Consistent with the increased water demand required for standard consistency, the workability of concrete mixes containing RHA exhibited a progressive decline, as reflected by reduced slump values. The maximum slump reduction—57.3%—occurred at the 25% replacement level, underscoring the need for plasticizers when incorporating biochar into concrete to maintain adequate workability.

4. Optimal cement replacement with RHA powder resulted in moderate enhancements in both compressive and tensile strength. The optimum replacement levels were identified as 10% for compressive strength and 15% for tensile strength, yielding improvements of 13.74% and 9.48%, respectively. These strength gains stem from the favorable chemical composition and pozzolanic reactivity of RHA, wherein its interaction with calcium hydroxide leads to the formation of additional C–S–H gel, thereby increasing bond strength. Additionally, the fine RHA particles contribute to a denser cement matrix by filling micro voids and refining pore structure, which collectively enhance the overall mechanical performance of the concrete.

5. X ray diffraction (XRD) analysis revealed a reduction in portlandite formation and an increase in C–S–H at the 10% and 15% replacement levels, indicating improved hydration behavior and enhanced pozzolanic activity relative to the control sample.

6. Energy dispersive X ray (EDX) analysis demonstrated a strong correlation between the Ca/Si ratio and compressive strength. In general, lower Ca/Si ratios corresponded to higher compressive strength, although the relationship was not strictly linear. The 10% RHA sample, which exhibited the lowest Ca/Si ratio, achieved the highest compressive strength, further supporting this trend.

7. Gamma ray attenuation testing indicated a modest improvement in the shielding performance of the concrete. The 15RHA sample exhibited a higher linear attenuation coefficient than the other mixes, primarily due to its increased density. Conversely, the 25RHA sample demonstrated inferior shielding performance.

8. The 15RHA sample recorded the highest fast neutron removal cross section (0.090 cm^{-1}) and the lowest values for HVLFCS (7.699 cm) and λFCS (11.107 cm), confirming its effectiveness and suitability as a neutron shielding material.

The 15RHA sample exhibited the highest fast neutron removal cross‑section (0.090 cm^{-1}) and the lowest HVLFCS (7.699 cm) and λFCS (11.107 cm), confirming its effectiveness and suitability as a neutron‑shielding material. Based on these findings, the biochar employed in this study—characterized by its distinctive chemical composition—demonstrated strong potential as an eco‑friendly cement replacement material, aligning well with sustainability objectives. This suitability arises from its capacity to reduce cement consumption, lower CO_2 emissions, and function as a medium for carbon sequestration.

Building upon the outcomes of this study, several promising avenues for future research can be pursued to further expand the application of this RHA. These include evaluating its influence on the structural performance of various concrete elements, such as beams, slabs, and columns. Additionally, the behavior of biochar‑modified concrete under extreme environmental conditions, including elevated temperatures and chemical exposure, warrants detailed investigation, alongside comprehensive long‑term durability assessments. Finally, exploring the use of this RHA in other concrete systems—such as high‑strength concrete, ultra‑high‑performance concrete, lightweight concrete, and heavyweight concrete—represents a valuable direction for future study.

References

[1] Akhtar, A., & Sarmah, A. K. (2018). Novel biochar-concrete composites: Manufacturing, characterization and evaluation of the mechanical properties. Science of the Total Environment, 616, 408-416. https://doi.org/10.1016/j.scitotenv.2017.10.319

[2] Zhang, Z., & Wang, B. (2016). Research on the life-cycle CO2 emission of China's construction sector. Energy and Buildings, 112, 244-255. https://doi.org/10.1016/j.enbuild.2015.12.026

[3] Senadheera, S. S., Gupta, S., Kua, H. W., Hou, D., Kim, S., Tsang, D. C. W., & Ok, Y. S. (2023). Application of biochar in concrete – A review. Cement and Concrete Composites, 143, 105204. https://doi.org/10.1016/j.cemconcomp.2023.105204

[4] Ataeifar, A., et al. (2025). Mechanical performance and freeze–thaw durability of expansive clay stabilized with graphene oxide and fly ash: A laboratory study.

[5] Yaashikaa, P. R., Kumar, P. S., Varjani, S., & Saravanan, A. (2020). A critical review on the biochar production techniques, characterization, stability and applications for circular bioeconomy. Biotechnology Reports, 28, e00570. https://doi.org/10.1016/j.btre.2020.e00570

[6] Shaheen, S. M., Niazi, N. K., Hassan, N. E. E., Bibi, I., Wang, H., Tsang, D. C. W., ... & Rinklebe, J. (2019). Wood-based biochar for the removal of potentially toxic elements in water and wastewater: a critical review. International Materials Reviews, 64(4), 216-247. https://doi.org/10.1080/09506608.2018.1473096

[7] Oladele, S. O., Adeyemo, A. J., & Awodun, M. A. (2019). Influence of rice husk biochar and inorganic fertilizer on soil nutrients availability and rain-fed rice yield in two contrasting soils. Geoderma, 336, 1-11. https://doi.org/10.1016/j.geoderma.2018.08.025

[8] Wakudkar, H., & Jain, S. (2022). A holistic overview on corn cob biochar: A mini-review. Waste Management & Research, 40(8), 1143-1155. https://doi.org/10.1177/0734242X211069741

[9] Odega, C. A., Ayodele, O. O., Ogutuga, S. O., Anguruwa, G. T., Adekunle, A. E., & Falconede, C. O. (2023). Potential application and regeneration of bamboo biochar for wastewater treatment: A review. Advances in Bamboo Science, 2, 100012. https://doi.org/10.1016/j.bamboo.2023.100012

[10] Ajien, A., Idris, J., Md Sofwan, N., Husen, R., & Seli, H. (2023). Coconut shell and husk biochar: A review of production and activation technology, economic, financial aspect and application. Waste Management & Research, 41(1), 37-51. https://doi.org/10.1177/0734242X221127167

[11] Maljaee, H., Madadi, R., Paiva, H., Tarelho, L., & Ferreira, V. M. (2021). Incorporation of biochar in cementitious materials: A roadmap of biochar selection. Construction and Building Materials, 283, 122757. https://doi.org/10.1016/j.conbuildmat.2021.122757

[12] Barbhuiya, S., Das, B. B., & Kanavaris, F. (2024). Biochar-concrete: A comprehensive review of properties, production and sustainability. Case Studies in Construction Materials, 20, e02859.

[13] Sun, Y., Gao, B., Yao, Y., Fang, J., Zhang, M., Zhou, Y., ... & Yang, L. (2014). Effects of feedstock type, production method, and pyrolysis temperature on biochar and hydrochar properties. Chemical Engineering Journal, 240, 574-578. https://doi.org/10.1016/j.cej.2013.10.081

[14] Alizadeh, A. (2017). A review of the effect of the behavior of core diameter varying H/D ratio on concrete core strength. Journal of Civil Engineering Researchers, 1(5), 42-45.

[15] Mansourghanaei, M., & Biklaryan, M. (2022). Experimental study of compressive strength, permeability and impact testing in geopolymer concrete based on blast furnace slag. Journal of Civil Engineering Researchers, 4(3), 31-39. https://doi.org/10.52547/JCER.4.3.31

[16] Mansourghanaei, M., & Biklaryan, M. (2022). Experimental evaluation of compressive, tensile strength and impact test in blast furnace slag based geopolymer concrete, under high temperature. Journal of Civil Engineering Researchers, 4(2), 12-21.

[17] Muthukrishnan, S., Gupta, S., & Kua, H. W. (2019). Application of rice husk biochar and thermally treated low silica rice husk ash to improve physical properties of cement mortar. Theoretical and Applied Fracture Mechanics, 104, 102376. https://doi.org/10.1016/j.tafmec.2019.102376

[18] Javed, M. H., Sikandar, M. A., Ahmad, W., Bashir, M. T., Alrowais, R., & Wadud, M. B. (2022). Effect of various biochars on physical, mechanical, and microstructural characteristics of cement pastes and mortars. Journal of Building Engineering, 57, 104850. https://doi.org/10.1016/j.jobe.2022.104850

[19] Gupta, S., Kua, H. W., & Pang, S. D. (2020). Effect of biochar on mechanical and permeability properties of concrete exposed to elevated temperature. Construction and Building Materials, 234, 117338. https://doi.org/10.1016/j.conbuildmat.2019.117338

[20] Ahmad, M. R., Chen, B., & Duan, H. (2020). Improvement effect of pyrolyzed agro-food biochar on the properties of magnesium phosphate cement. Science of the Total Environment, 718, 137422. https://doi.org/10.1016/j.scitotenv.2020.137422

[21] Qin, Y., Pang, X., Tan, K., & Bao, T. (2021). Evaluation of pervious concrete performance with pulverized biochar as cement replacement. Cement and Concrete Composites, 119, 104022. https://doi.org/10.1016/j.cemconcomp.2021.104022

[22] Sirico, A., Belletti, B., Bernardi, P., Malcevschi, A., Pagliari, F., Fornoni, P., & Moretti, E. (2022). Effects of biochar addition on long-term behavior of concrete. Theoretical and Applied Fracture

Mechanics, 122, 103626. https://doi.org/10.1016/j.tafmec.2022.103626
[23] Liu, W., Li, K., & Xu, S. (2022). Utilizing bamboo biochar in cement mortar as a bio-modifier to improve the compressive strength and crack-resistance fracture ability. Construction and Building Materials, 327, 126917. https://doi.org/10.1016/j.conbuildmat.2022.126917
[24] Ling, Y., Wu, X., Tan, K., & Zou, Z. (2023). Effect of biochar dosage and fineness on the mechanical properties and durability of concrete. Materials, 16(7), 2809. https://doi.org/10.3390/ma16072809
[25] Qing, L., Zhang, H., & Zhang, Z. (2023). Effect of biochar on compressive strength and fracture performance of concrete. Journal of Building Engineering, 78, 107587. https://doi.org/10.1016/j.jobe.2023.107587
[26] Jia, Y., Li, H., He, X., Li, P., & Wang, Z. (2023). Effect of biochar from municipal solid waste on mechanical and freeze–thaw properties of concrete. Construction and Building Materials, 368, 130374. https://doi.org/10.1016/j.conbuildmat.2023.130374
[27] Pang, X., Qin, Y., Wei, P., & Huang, C. (2024). Enhancing fire resistance: Investigating mechanical properties of biochar-infused concrete under elevated temperatures. Construction and Building Materials, 435, 136813. https://doi.org/10.1016/j.conbuildmat.2024.136813
[28] Mekky, K. M., Ibrahim, M. G., Sharobim, K., Fujii, M., & Nasr, M. (2024). Evaluating environmental and economic benefits of using biochar in concrete: A life cycle assessment and multi-criteria decision-making framework. Case Studies in Construction Materials, 21, e03712. https://doi.org/10.1016/j.cscm.2024.e03712
[29] Hylton, J., Hugen, A., Rowland, S. M., Griffin, M., & Tunstall, L. E. (2024). Relevant biochar characteristics influencing compressive strength of biochar-cement mortars. Biochar, 6(1), 1-27. https://doi.org/10.1007/s42773-024-00375-6
[30] Wang, T., Tang, Y., Qin, S., Li, G., Wu, H., & Leung, C. K. Y. (2025). Sustainable and mechanical properties of engineered cementitious composites with biochar: Integrating micro- and macro-mechanical insight. Cement and Concrete Composites, 155, 105813. https://doi.org/10.1016/j.cemconcomp.2024.105813
[31] ASTM C150/C150M. (2001). Standard specification for Portland cement. ASTM International. https://doi.org/10.1520/C0150_C0150M-21
[32] ASTM C188. (2009). Standard test method for density of hydraulic cement. ASTM International.
[33] EN 196-1. (2005). Methods of testing cement – Part 1: Determination of strength. European Committee for Standardization. https://doi.org/10.3403/30291447
[34] ASTM C109/C109M. (2011). Standard test method for compressive strength of hydraulic cement mortars. ASTM International. https://doi.org/10.1520/c0109_c0109m-13e01
[35] Nimmo, J. R., & Perkins, K. S. (2002). Aggregate stability and size distribution. In Methods of Soil Analysis: Part 4 Physical Methods (Vol. 5, pp. 317-328). Soil Science Society of America.
[36] ASTM C136/C136M. (2006). Standard test method for sieve analysis of fine and coarse aggregates. ASTM International.
[37] BS 812-110. (1990). Testing aggregates – Part 110: Methods for determination of aggregate crushing value (ACV). BSI, UK.
[38] ASTM C128. (2012). Standard test method for density, relative density (specific gravity), and absorption of fine aggregate. ASTM International. https://doi.org/10.1520/C0128-22
[39] ASTM C29/C29M. (2009). Standard test method for bulk density ("unit weight") and voids in aggregate. ASTM International.
[40] ASTM C142/C142M. (1998). Standard test method for clay lumps and friable particles in aggregates. ASTM International.
[41] Kucche, K. J., Jamkar, S. S., & Sadgir, P. A. (2015). Quality of water for making concrete: a review of literature. International Journal of Scientific and Research Publications, 5(1), 1-10. https://doi.org/10.12691/ajcea-7-2-1
[42] Christensen, B. J., & Farzam, H. (2006). Chemical admixtures. In Significance of Tests and Properties of Concrete and Concrete-Making Materials (pp. 484-494). ASTM International. https://doi.org/10.1520/stp37760s
[43] Dehkhoda, A. M., Ellis, N., & Gyenge, E. (2014). Electrosorption on activated biochar: effect of thermo-chemical activation treatment on the electric double layer capacitance. Journal of Applied Electrochemistry, 44, 141-157. https://doi.org/10.1007/s10800-013-0636-1
[44] Kang, X., Kang, G.-C., & Ge, L. (2013). Modified time of setting test for fly ash paste and fly ash–soil mixtures. Journal of Materials in Civil Engineering, 25(2), 296-301. https://doi.org/10.1061/(asce)mt.1943-5533.0000604
[45] ASTM C157/C157M. (2010). Standard test method for length change of hardened hydraulic-cement mortar and concrete. ASTM International.
[46] Al-Saleh, W. M., Almutairi, H. M., Sayyed, M. I., & Elsafi, M. (2024). A comprehensive study of the shielding ability from ionizing radiation of different mortars using iron filings and bismuth oxide. Scientific Reports, 14(1), 10014. https://doi.org/10.1038/s41598-024-60188-2
[47] El-Samrah, M. G., Nabil, I. M., Shamekh, M. E., Elmasry, M., & Osman, M. (2024). Microstructure and radiation shielding capabilities of Al-Cu and Al-Mn alloys. Scientific Reports, 14(1), 26721. https://doi.org/10.1038/s41598-024-76177-4
[48] Singh, V., Shirmardi, S. P., Medhat, M. E., & Badiger, N. M. (2015). Determination of mass attenuation coefficient for some polymers using Monte Carlo simulation. Vacuum, 119, 284-288. https://doi.org/10.1016/j.vacuum.2015.06.006
[49] Al-Ghamdi, H., Alsaif, N. A. M., Alfryyan, N., Rammah, Y. S., & Nabil, I. M. (2024). Investigation of gamma-ray and neutron protection competence of oxyfluoride aluminosilicate glasses reinforced with TbF3: Comparative study. Radiation Physics and Chemistry, 112105. https://doi.org/10.1016/j.radphyschem.2024.112105
[50] Şakar, E., Han, İ., Arslan, İ., & Singh, V. (2020). Phy-X/PSD: Development of a user friendly online software for calculation of parameters relevant to radiation shielding and dosimetry. Radiation Physics and Chemistry, 166, 108496.
[51] Mahmoud, A. A., Abouelnour, M. A., Fathy, I. N., Alturki, M., & Abdelaziz, M. (2024). Influence of sustainable waste granite, marble and nano-alumina additives on ordinary concretes: a physical, structural, and radiological study. Scientific Reports, 14(1), 22011.
[52] Fathy, I. N., El-Sayed, A. A., Elfakharany, M. E., Mahmoud, A. A., Mohamed, A. A., & Mahmoud, A. S. (2024). Enhancing mechanical properties and radiation shielding of high-strength concrete with bulk lead oxide and granodiorite. Nuclear Engineering and Design, 429, 113626. https://doi.org/10.1016/j.nucengdes.2024.113626
[53] Fathy, I. N., El-Sayed, A. A., Elfakharany, M. E., Mahmoud, A. A., Mohamed, A. A., & Mahmoud, A. S. (2025). Upgrading the compressive strength and radiation shielding properties of high strength concrete supported with nano additives of lead monoxide and granodiorite. Progress in Nuclear Energy, 180, 105562.
[54] Gupta, S., Kua, H. W., & Low, C. Y. (2018). Use of biochar as carbon sequestering additive in cement mortar. Cement and Concrete Composites, 87, 110-129. https://doi.org/10.1016/j.cemconcomp.2017.12.009
[55] Akinyemi, B. A., & Adesina, A. (2020). Recent advancements in the use of biochar for cementitious applications: A review. Journal of Building Engineering, 32, 101705. https://doi.org/10.1016/j.jobe.2020.101705

[56] Wang, L., Chen, L., Tsang, D. C. W., Kua, H. W., Yang, J., Ok, Y. S., ... & Poon, C. S. (2019). The roles of biochar as green admixture for sediment-based construction products. Cement and Concrete Composites, 104, 103348. https://doi.org/10.1016/j.cemconcomp.2019.103348

[57] Murali, G., & Wong, L. S. (2024). A comprehensive review of biochar-modified concrete: Mechanical performance and microstructural insights. Construction and Building Materials, 425, 135986.

[58] Gupta, S., Kua, H. W., & Pang, S. D. (2018). Biochar-mortar composite: Manufacturing, evaluation of physical properties and economic viability. Construction and Building Materials, 167, 874-889. https://doi.org/10.1016/j.conbuildmat.2018.02.104

[59] Gomes, S. D. C., Zhou, J. L., Zeng, X., & Long, G. (2022). Water treatment sludge conversion to biochar as cementitious material in cement composite. Journal of Environmental Management, 306, 114463. https://doi.org/10.1016/j.jenvman.2022.114463

[60] Yang, X., & Wang, X.-Y. (2021). Hydration-strength-durability-workability of biochar-cement binary blends. Journal of Building Engineering, 42, 103064. https://doi.org/10.1016/j.jobe.2021.103064

[61] Siddique, S., Shrivastava, S., & Chaudhary, S. (2018). Influence of ceramic waste as fine aggregate in concrete: Pozzolanic, XRD, FT-IR, and NMR investigations. Journal of Materials in Civil Engineering, 30(9), 04018227. https://doi.org/10.1061/(asce)mt.1943-5533.0002438

[62] Thomas, M., et al. (2008). Diagnosing delayed ettringite formation in concrete structures. Cement and Concrete Research, 38(6), 841-847.

[63] Kim, J. J., Foley, E. M., & Taha, M. M. R. (2013). Nano-mechanical characterization of synthetic calcium–silicate–hydrate (C–S–H) with varying CaO/SiO2 mixture ratios. Cement and Concrete Composites, 36, 65-70.

[64] Choudhary, R., et al. (2021). Mechanical and abrasion resistance performance of silica fume, marble slurry powder, and fly ash amalgamated high strength self-consolidating concrete. Construction and Building Materials, 269, 121282.

[65] Dadsetan, S., & Bai, J. (2017). Mechanical and microstructural properties of self-compacting concrete blended with metakaolin, ground granulated blast-furnace slag and fly ash. Construction and Building Materials, 146, 658-667.

[66] Abouelnour, M. A., Fathy, I. N., Mahmoud, A. A., Alturki, M., & Abdelaziz, M. (2024). Recycling of marble and granite waste in concrete by incorporating nano alumina. Construction and Building Materials, 411, 134456. https://doi.org/10.1016/j.conbuildmat.2023.134456

[67] Fathy, I. N., Elfakharany, M. E., & El-Sayed, A. A. (2024). Recycling of waste granodiorite powder as a partial cement replacement material in ordinary concrete. Advances in Materials Science, 24(3), 56-88.

[68] El-Samrah, M., et al. (2022). Radiation shielding properties of modified concrete mixes and their suitability in dry storage cask. Progress in Nuclear Energy, 148, 104195.

[69] Kassem, S. M., et al. (2023). Optical and radiation shielding properties of PVC/BiVO4 nanocomposite. Scientific Reports, 13(1), 10964. https://doi.org/10.1038/s41598-023-37916-7

[70] Saleh, A., et al. (2024). The role of MoO3 on the physical, elasto-mechanical and nuclear shielding efficiency of barium-boro-bismuthate glass system: Comparative investigation. Materials Chemistry and Physics, 129574.

[71] Ekinci, N., et al. (2022). Impacts of the colemanite on the enhancement of the radiation shielding capacity of polypropylene. Journal of Materials Science: Materials in Electronics, 33(25), 20046-20055. https://doi.org/10.1007/s10854-022-08803-w

[72] Al-Ghamdi, H., et al. (2024). Investigation of gamma-ray and neutron protection competence of oxyfluoride aluminosilicate https://doi.org/10.1016/j.radphyschem.2024.112105

[73] Kaky, K. M., et al. (2020). Theoretical and experimental validation gamma shielding properties of B2O3–ZnO–MgO–Bi2O3 glass system. Materials Chemistry and Physics, 242, 122504. https://doi.org/10.1016/j.matchemphys.2019.122504

[74] Japari, S., et al. (2021). Effects of Na2O on optical and radiation shielding properties of xNa2O-(20-x)K2O-30V2O5-50TeO2 mixed alkali glasses. Results in Physics, 22, 103946. https://doi.org/10.1016/j.rinp.2021.103946

[75] Kiran, K., et al. (2015). Effective atomic number of selected construction materials using gamma backscattering technique. Annals of Nuclear Energy, 85, 1077-1084.

[76] Martellucci, R., & Torsello, D. (2022). Potential of biochar reinforced concrete as neutron shielding material. Nuclear Engineering and Technology, 54(9), 3448-3451. https://doi.org/10.1016/j.net.2022.03.022

[77] Yasir, M., et al. (2020). Shielding properties of cement composites filled with commercial biochar. Electronics, 9(5), 819. https://doi.org/10.3390/electronics9050819